Retina

The Project MACULA Retinal Pigment Epithelium Grading System for Histology and Optical Coherence Tomography in Age-Related Macular Degeneration

Emma C. Zanzottera,[1,2] Jeffrey D. Messinger,[1] Thomas Ach,[1,3] R. Theodore Smith,[4] K. Bailey Freund,[4–6] and Christine A. Curcio[1]

[1]Department of Ophthalmology, University of Alabama School of Medicine, Birmingham, Alabama, United States
[2]Eye Clinic, Department of Clinical Science "Luigi Sacco," Sacco Hospital, University of Milan, Milan, Italy
[3]University Hospital Würzburg, Department of Ophthalmology, Würzburg, Germany
[4]Department of Ophthalmology, New York University School of Medicine, New York City, New York, United States
[5]Vitreous Retina Macula Consultants of New York, New York, New York, United States
[6]LuEsther T. Mertz Retinal Research Center, Manhattan Eye, Ear, and Throat Hospital, New York, New York, United States

Correspondence: Christine A. Curcio, Department of Ophthalmology, EyeSight Foundation of Alabama Vision Research Laboratories, 1670 University Boulevard Room 360; University of Alabama School of Medicine, Birmingham, AL 35294-0099, USA;
curcio@uab.edu.

Submitted: January 11, 2015
Accepted: March 17, 2015

Citation: Zanzottera EC, Messinger JD, Ach T, Smith RT, Freund KB, Curcio CA. The Project MACULA retinal pigment epithelium grading system for histology and optical coherence tomography in age-related macular degeneration. *Invest Ophthalmol Vis Sci*. 2015;56:3253–3268.
DOI:10.1167/iovs.15-16431

Purpose. To seek pathways of retinal pigment epithelium (RPE) fate in age-related macular degeneration via a morphology grading system; provide nomenclature, visualization targets, and metrics for clinical imaging and model systems.

Methods. Donor eyes with geographic atrophy (GA) or choroidal neovascularization (CNV) and one GA eye with previous clinical spectral-domain optical coherence tomography (SDOCT) imaging were processed for histology, photodocumented, and annotated at predefined locations. Retinal pigment epithelial cells contained spindle-shaped melanosomes, apposed a basal lamina or basal laminar deposit (BLamD), and exhibited recognizable morphologies. Thicknesses and unbiased estimates of frequencies were obtained.

Results. In 13 GA eyes (449 locations), 'Shedding,' 'Sloughed,' and 'Dissociated' morphologies were abundant; 22.2% of atrophic locations had 'Dissociated' RPE. In 39 CNV eyes (1363 locations), 37.3% of locations with fibrovascular/fibrocellular scar had 'Entombed' RPE; 'Sloughed,' 'Dissociated,' and 'Bilaminar' morphologies were abundant. Of abnormal RPE, CNV and GA both had ~35% 'Sloughed'/'Intraretinal,' with more Intraretinal in CNV (9.5% vs. 1.8%). 'Shedding' cells associated with granule aggregations in BLamD. The RPE layer did not thin, and BLamD remained thick, with progression. Granule-containing material consistent with three morphologies correlated to SDOCT hyperreflective foci in the previously examined GA patient.

Conclusions. Retinal pigment epithelium morphology indicates multiple pathways in GA and CNV. Atrophic/scarred areas have numerous cells capable of transcribing genes and generating imaging signals. Shed granule aggregates, possibly apoptotic, are visible in SDOCT, as are 'Dissociated' and 'Sloughed' cells. The significance of RPE phenotypes is addressable in longitudinal, high-resolution imaging in clinic populations. Data can motivate future molecular phenotyping studies.

Keywords: age-related macular degeneration, retinal pigment epithelium, melanosomes, lipofuscin, histology, apoptosis, migration, transdifferentiation, basal laminar deposits, spectral-domain optical coherence tomography

Age-related macular degeneration (AMD) causes worldwide vision loss, at a high social and economic cost.[1–3] A disease of the photoreceptor support system,[4] AMD's pathology is prominent in the retinal pigment epithelium (RPE) and underlying Bruch's membrane (BrM). The RPE is a monolayer of cuboidal epithelial cells of neuroectodermal origin, dually tasked with maintaining retina apically and choroid basally.[5–7] In AMD, internal to the RPE basement membrane is basal laminar deposit (BLamD),[8] a thickened layer of extracellular matrix proteins secreted by RPE and associated with disease progression.[9] External to the RPE basement membrane are extracellular drusen and basal linear deposits[10] that in vivo separate outer retinal cells from vasculature and promote neovascularization; these also are synthesized by RPE. Pigmentary and autofluorescence variations represent clinically detectable RPE decompensation and disease progression.[11,12] The RPE is thus a key AMD participant, victim, and reporter of clinically inconspicuous events in BrM.

High-resolution clinical imaging reveals the cellular basis of disease progression as never before.[13] Clinically deployed and experimental technologies show the RPE en face[14–19] and in cross section with other chorioretinal layers.[20,21] A research priority is identifying novel anatomic biomarkers derived from spectral-domain optical coherence tomography (SDOCT),[22] including components of the hyperreflective band attributed to RPE and BrM. The RPE is revealed in vivo by its abundant

melanosomes, melanolipofuscin, and lipofuscin granules, all of lysosomal lineage[23–25] and all potential subcellular contributors to SDOCT reflectivity.[26,27] Yet RPE imaging relies on surprisingly few data about the number, size, shape, and disposition of individual RPE cells and their organelles of imaging significance. Previous morphological studies of RPE in AMD and Stargardt disease, an inherited disorder also featuring abundant RPE lipofuscin, collectively used low-resolution light microscopy, electron microscopy of small series, minimally characterized or insufficiently advanced pathology, and imprecisely specified retinal localizations.[28–38] This knowledge gap impedes the full exploitation of RPE-centered imaging technologies.

We hypothesize that the RPE exhibits stereotypic stress responses and death pathways, which if defined, quantified, and followed, provide windows into molecular pathology and points of therapeutic entry. Like others we used grading systems to discretize RPE morphology, compare across eyes and retinal regions, and facilitate quantification.[31–33,39–43] Using this approach, we proposed two main pathways: apical (sloughing into subretinal space and intraretinal migration) versus basal (shedding of granules into subjacent BLamD).[32] In this report, we describe, illustrate, and account for morphologies of RPE cells in geographic atrophy (GA) and choroidal neovascularization (CNV), the two AMD end stages, using melanosomes, lipofuscin, and BLamD as anatomical markers. A companion report[44] focuses on RPE-derived cells, that is, out-of-RPE layer cells containing melanosomes and lacking contact with BLamD. We estimate the frequency of RPE morphologies, quantify RPE and BLamD thicknesses, determine if RPE morphologies are visible by SDOCT, and propose testable hypotheses about RPE fate in AMD, where fates include death, conversion to a cell type not meeting criteria for RPE, and emigration. Collectively, our data support multiple modes of RPE stress response; provide nomenclature, visualization targets, and metrics for clinical imaging and experimental systems; and motivate future molecular phenotyping studies.

Methods

This study was approved by the Institutional Review Board at the University of Alabama at Birmingham and the North Shore-LIJ Health System, Inc. It complied with the Health Insurance Portability and Accountability Act and the Declaration of Helsinki.

Tissue Preparation

Tissues were accessioned, evaluated, and processed for macula-wide, submicrometer sections, as previously described[8,43,45] and with additional details in the Supplementary Material, including links to digital sections from which figures were chosen.

Annotation and Layer Thickness Measurements

To permit unbiased estimates for the frequency of each morphology, we annotated sections at locations chosen using systematic sampling. As described previously,[43] we employed a custom ImageJ plug-in (http://imagej.nih.gov/ij/; provided in the public domain by the National Institutes of Health, Bethesda, MD, USA) that allowed the user to populate a database with classifications and layer thicknesses at predefined locations. Locations were pooled within each of two standard horizontal planes, 2 mm superior to the foveal center (Superior) and through the foveola and optic nerve (Central). Additional details are provided in the Supplementary Material. Frequencies expressed as a function of distance from defined borders in GA and CNV eyes[32,33,46,47] will be reported separately.

We defined RPE as cells containing RPE melanosomes and lipofuscin, internal to basal lamina or BLamD, if present, or BrM if not.[48] We defined RPE-derived cells as those with RPE melanosomes and lipofuscin, not adjacent to basal lamina or BLamD, and out of the RPE layer (see our companion paper).[44] Retinal pigment epithelium melanosomes are unique due to their spindle shape.[24] Lipofuscin granules are recognizable by their size (~1 μm), shape (irregular, potato-like), abundance, and polychromatic coloration imparted by toluidine blue (blue-green, tending toward bronze or brown depending on the eye). By referring to transmission electron microscopy (TEM), it was possible to discriminate melanosomes from the combined population of lipofuscin and melanolipofuscin (LF/MLF) granules (Supplementary Fig. S1).

The RPE layer was defined as the plane of RPE cells located between the subretinal and sub-RPE spaces, which are divided by the RPE if present and BLamD if not. Because the RPE layer is internal to BLamD, which can outlast cells in advanced AMD, the plane of the RPE layer can be defined when cells are absent.[8,48] For our grading system we used the term "epithelial" for a continuous cellular layer with junctional complexes linking individual RPE cells to each other. We used the term "nonepithelial" for a noncontinuous layer of cells containing RPE melanosomes and for RPE cells and cellular material not adjacent to basal lamina or BLamD. In Table 1, three RPE grades contain epithelial and nonepithelial components. Four are epithelial only. Two are nonepithelial only. The term "atrophy" signifies absence of pigmented cells.

Retinal pigment epithelium layer thicknesses were measured perpendicular to BrM and excluded apical processes. Thicknesses were recorded where the RPE layer was continuous, including the epithelial components of grades 'Sloughed,' 'Shedding,' and 'Intraretinal,' as defined in Table 1 and described in Results, as well as continuous layers of Entombed in selected locations (additional details in Supplementary Material). In atrophic areas, RPE thickness was set to zero. For thickness measurements, BLamD was identified as previously described,[8] and both early and late forms were included, if present. Definitions and procedures for nonepithelial cells and BLamD are included in the Supplementary Material. Thicknesses measured for RPE and BLamD were each compared between Superior and Central sections, separately in GA and CNV eyes, and then combined because findings were consistent. Because some RPE phenotypes were found very rarely, detailed statistical analysis among grades was not possible.

Clinicopathologic Correlation

As previously described,[49] a 98-year-old white woman had nonneovascular AMD with subretinal drusenoid deposits (left eye), an acquired vitelliform lesion that collapsed by March 2011 leaving central GA (right eye), pigmentary changes (both eyes), and absence of typical small or large drusen but presence of histologically detectable basal linear deposit and abundant BLamD (both eyes). She underwent multimodal clinical imaging including SDOCT in April 2013 and died in December 2013. Eyes were recovered at 8:55 hours post mortem, preserved, and processed as described above. A sub-RPE neovascularization discovered on histology was likely present and quiescent during the vitelliform collapse. Eye tracking software (Spectralis, Heidelberg Engineering, Heidelberg, Germany) was used to align in vivo and ex vivo SDOCT scans.[49] Histologic sections matched to the scans were digitized using image-stitching software (CellSens; Olympus, Center Valley, PA, USA) and a ×20 planapochromat objective. Correspondences between histology and SDOCT were verified

Table 1. Definitions of RPE Cell and RPE Layer Morphologies; RPE Frequencies and Thicknesses in GA and CNV Eyes

Morphology*	Cell	Layer Components†	Description‡	Geographic Atrophy, Superior + Central		Choroidal Neovascularization, Superior + Central	
				Frequency No.; %	Thickness Mean ± SD, µm	Frequency No.; %	Thickness Mean ± SD, µm
'Nonuniform'	RPE	Epithelial	Slightly nonuniform morphology and pigmentation	80; 17.8	11.7 ± 2.6	36; 2.6	10.9 ± 2.4
'Very Nonuniform'	RPE	Epithelial	Very nonuniform morphology and pigmentation	143; 31.8	10.0 ± 3.9	189; 13.9	10.7 ± 3.8
'Sloughed'	RPE	Epithelial, nonepithelial	Intact epithelium with spherical cells sloughed into subretinal space	38; 8.5	17.0 ± 8.1	44; 3.2	18.9 ± 9.9
'Shedding'	RPE	Epithelial, nonepithelial	Intact epithelium with basal shedding of nonnucleated granule aggregates into BLamD	39; 8.7	13.0 ± 3.9	25; 1.8	10.9 ± 4.8
'Bilaminar'	RPE	Epithelial	Double layers	2; 0.4	19.5 ± 2.4	37; 2.7	17.8 ± 6.8
'Vacuolated'	RPE	Epithelial	A single large vacuole, sometimes with contents, delimited apically by extremely effaced cytoplasm	1; 0.2	28.1	5; 0.4	17.4 ± 9.2
'Intraretinal'	RPE	Epithelial, nonepithelial	Nucleated RPE in neurosensory retina, anterior to external limiting membrane	2; 0.4	10.3 ± 7.2	16; 1.2	11.6 ± 4.1
'Dissociated'	RPE	Nonepithelial	Nucleated individual RPE in an atrophic area lacking an external limiting membrane, distinguishing this grade from 'Intraretinal'	32; 7.1	Not measured	41; 3.0	Not measured
'Entombed'	RPE	Nonepithelial	Entombed by fibrovascular/fibrocellular scar, intermingled with other cells and fluid in the same plane	n.a.	n.a.	302; 22.2	16.6 ± 10.6
'Atrophy with BLamD'	Atrophy	Atrophy	No pigmented cells; persistent BLamD	86; 19.3	0	402; 29.5	0
'Atrophy without BLamD'	Atrophy	Atrophy	No pigmented cells; no BLamD	26; 5.8	0	266; 19.5	0
Total				449; 100		1363; 100	

n.a., not available; 'Entombed' RPE are found in neovascular AMD eyes only.

* Verbal descriptors replace numbered grades used in our previous publications[32,33] and at http://projectmacula: 'Nonuniform,' 1; 'Very Nonuniform,' 2; 'Sloughed,' 2A; 'Shedding,' 2B; 'Bilaminar,' 2L; 'Intraretinal,' 3; 'Atrophy with BLamD,' 4; 'Atrophy without BLamD,' 5.

† Epithelial, continuous layer of RPE cells; nonepithelial, noncontinuous layer of RPE cells, not adjacent to basal lamina or BLamD.

‡ Three morphologies ('Subducted,' 'Melanotic,' and 'Entombed,' Fig. 1) are considered RPE derived and are presented in a companion paper.[44]

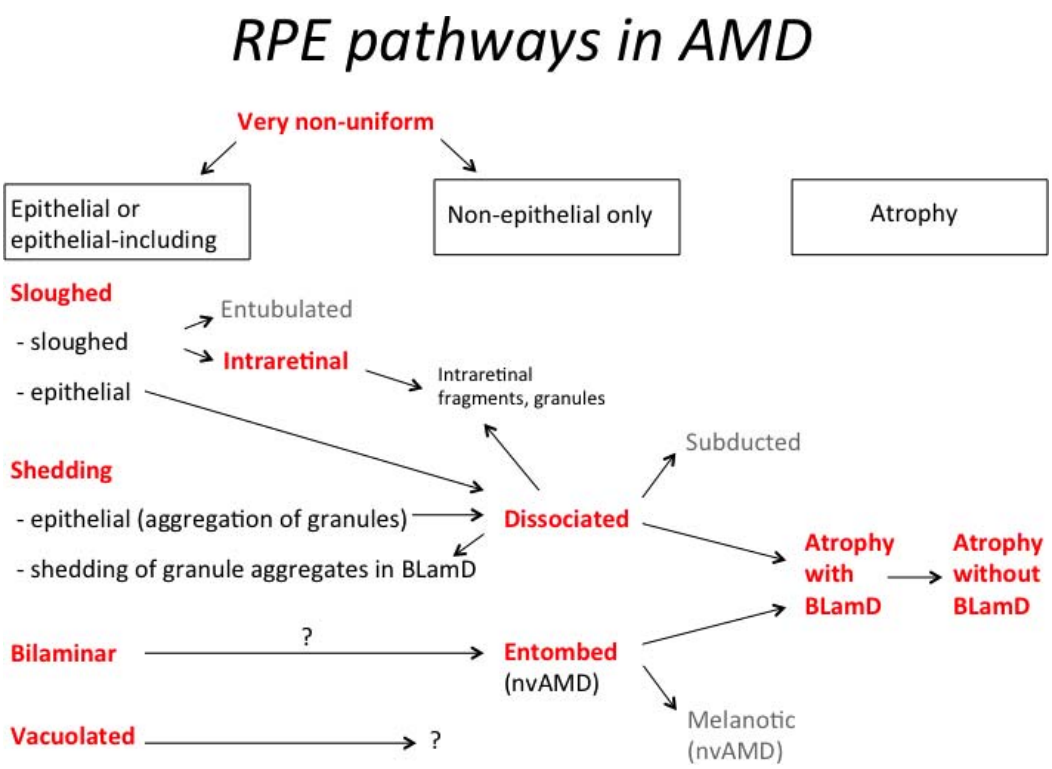

Figure 1. Graphical hypothesis of RPE pathways in AMD. The schema omits normal aging changes and begins with 'Very Nonuniform.' RPE cells proceed to more advanced epithelial and nonepithelial grades. Three RPE-derived morphologies (grayed out) are reported separately.[44,45] 'Dissociated' and 'Entombed' are the final steps before dissolution of the RPE layer (atrophy). 'Dissociated' cells likely give rise to cellular fragments and loose granules seen in the neurosensory retina. Direct and primary contributors to 'Dissociated' appear to be the epithelial components of 'Sloughed'/'Intraretinal' and 'Shedding.' 'Sloughed' RPE can become 'Intraretinal.' Some enter the lumen of outer retinal tubulation from the subretinal space.[45,147] The epithelial component of 'Shedding' contains intracellular granule aggregations,[52] less readily appreciated in histology, which are released into BLamD and may represent apoptotic bodies. The relationship between 'Bilaminar' and 'Entombed RPE' is hypothetical, and the fate of rare 'Vacuolated' RPE cells is unknown. The term atrophy does not specify the fate of individual cells. Death is one possible outcome. Alternatives are transition to a form that does not meet our criteria for RPE (e.g., loss of granules) and emigration.[44] Not all morphologies depigment; the principal ones are 'Entombed' and 'Subducted.'[44] nvAMD, neovascular AMD.

by comparing images of entire sections to scans, especially contours of the inner retinal surface and inner nuclear layer (INL)[50] horizontal extent of BLamD and split RPE-BrM band, and the external limiting membrane (ELM) terminations at the GA borders.[8] All scans and sections will be published in a report of neovascular changes in this eye. We use the terminology of Staurenghi et al.[51] for SDOCT bands.

Results

Our results are based on 52 human eyes from 51 donors with ex vivo imaging and histopathologic findings consistent with advanced AMD (Supplementary Table S1). A total of 1812 locations were evaluated in 13 eyes with GA (449 locations; 150 Superior and 299 Central) and 39 eyes with choroidal CNV (1363 locations; 452 Superior and 911 Central). To organize the results, Figure 1 is a graphical hypothesis that incorporates all RPE morphologies into pathways that are fully explained in the Discussion.

Table 1 lists cell and layer characteristics of RPE morphologies, and Figure 2 illustrates at higher resolution those previously described at lower resolution.[32,33,43] In older eyes, RPE is slightly 'Nonuniform' in size and pigmentation with BLamD (Fig. 2A), and many cells are 'Very Nonuniform' (Fig. 2B). 'Sloughed' and 'Intraretinal' morphologies both have epithelial components of cells overlying BLamD, plus anteriorly placed nonepithelial components: spherical cells desquamated into the subretinal space for 'Sloughed' (Fig. 2G), and cells anterior to an intact ELM for 'Intraretinal' (Fig. 2E). Density and composition of intracellular granules in the nonepithelial subretinal and intraretinal cells closely resemble those of epithelial cells. 'Intraretinal' is often seen near 'Sloughed' in the same[33] or nearby histologic sections, and we consider the two a pathogenic continuum. 'Shedding' RPE comprises an irregular epithelial layer associated with overlying shed, nonnucleated granule aggregates within a thick continuous BLamD (Fig. 2D). 'Bilaminar' RPE comprises double layers of epithelial RPE adherent to early BLamD (Fig. 2I), distinguishable from rearrangement due to damage in processing by the intact tissues around it and repeatability across specimens.[32,33,52] 'Vacuolated' RPE, newly added, have a single large vacuole delimited apically by extremely effaced cytoplasm (Fig. 2J). In 'Atrophy with BLamD,' RPE cells have died more recently than in 'Atrophic without BLamD' (Figs. 2H, 2K).

We next show examples of newly recognized nonepithelial morphologies (Figs. 2, 3, 4). 'Dissociated' RPE comprises separate spherical or ovoid cells with nuclei in the atrophic area (mean diameter 13.7 μm, Fig. 2C). 'Dissociated' RPE was found in degenerated outer nuclear layer in 25 locations (34.2%), in the Henle fiber layer in 44 locations (60.3%), and in foveal INL in 4 locations (5.5%). 'Dissociated' RPE differs from 'Intraretinal' by the absence of ELM and any epithelial RPE. Cells were adherent to BLamD (Figs. 3A, 3B), detached from BLamD (Fig. 3C), or adherent to BrM (Fig. 3D). Frequently, 'Dissociated' cells were accompanied by cellular fragments or

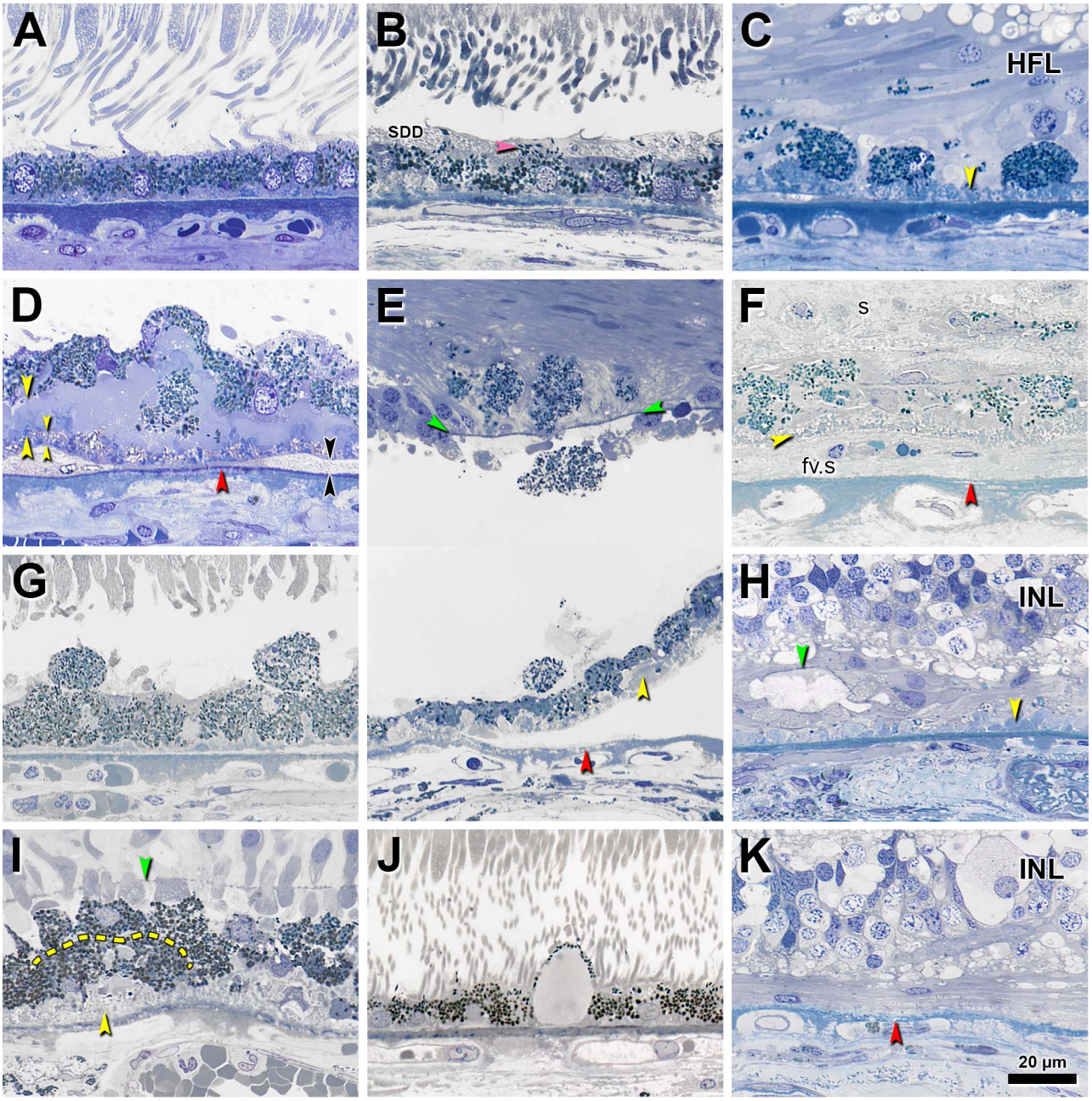

Figure 2. Grades of RPE morphology in late AMD. Submicrometer epoxy resin sections were stained with toluidine blue. Epithelial RPE and RPE morphologies with epithelial components (**A**, **B**, **D**, **E**, **G**, **I**, **J**); nonepithelial (noncontinuous) morphologies (**C**, **F**); atrophic RPE (**H**, **K**). (**A**) 'Nonuniform' RPE: slightly 'Nonuniform' morphology and pigmentation with small patches of early BLamD. (**B**) 'Very Nonuniform' RPE: more nonuniformity in shape and pigmentation; melanosomes within apical processes (*pink arrowhead*). Subretinal drusenoid deposits (SDD) localize to RPE apical aspect. (**C**) 'Dissociated' RPE: individual RPE cells with or without nuclei in atrophic area, adherent to early BLamD. Some RPE granules are translocated among HFL fibers. (**D**) 'Shedding' RPE: basal translocation of shed RPE fragments into a thick continuous layer of BLamD (late and early forms shown by *large* and *small yellow arrowheads*, respectively); BLinD (*black arrowheads*). (**E**) 'Intraretinal' RPE: anterior migration through ELM. Epithelial component remains atop BLamD (*bottom*), which in turn overlies an artifactually empty soft druse. Photoreceptors have degenerated. Retina is artifactually detached. (**F**) Cells 'Entombed' by a subretinal scar (s) together with nonpigmented cells. Persistent BLamD divides subretinal fibrocellular scar in the subretinal space from fibrovascular scar (fv.s) in sub-RPE space. (**G**) 'Sloughed' RPE: release of spherical cells into the subretinal space; the epithelial component overlies BLamD (*blue*) and BLinD (*gray*). (**H**) 'Atrophy with BLamD': absent RPE and persistent BLamD. Photoreceptors have atrophied. ELM delimits end-stage outer retinal tubulation.[45] (**I**) 'Bilaminar': double layers of epithelial RPE (delimited by *dotted line*) adherent to BLamD. (**J**) 'Vacuolated' RPE: cells with a single large vacuole delimited apically by extremely effaced cytoplasm. (**K**) 'Atrophy without BLamD': absent RPE, absent BLamD. Photoreceptors have atrophied. *Yellow arrowheads*: BLamD; *red arrowheads*: calcification in BrM; *green arrowheads*: ELM. BLamD, basal laminar deposits; BLinD, basal linear deposits; ELM, external limiting membrane; HFL, Henle fiber layer; INL, inner nuclear layer; RPE, retinal pigment epithelium.

Investigative Ophthalmology & Visual Science

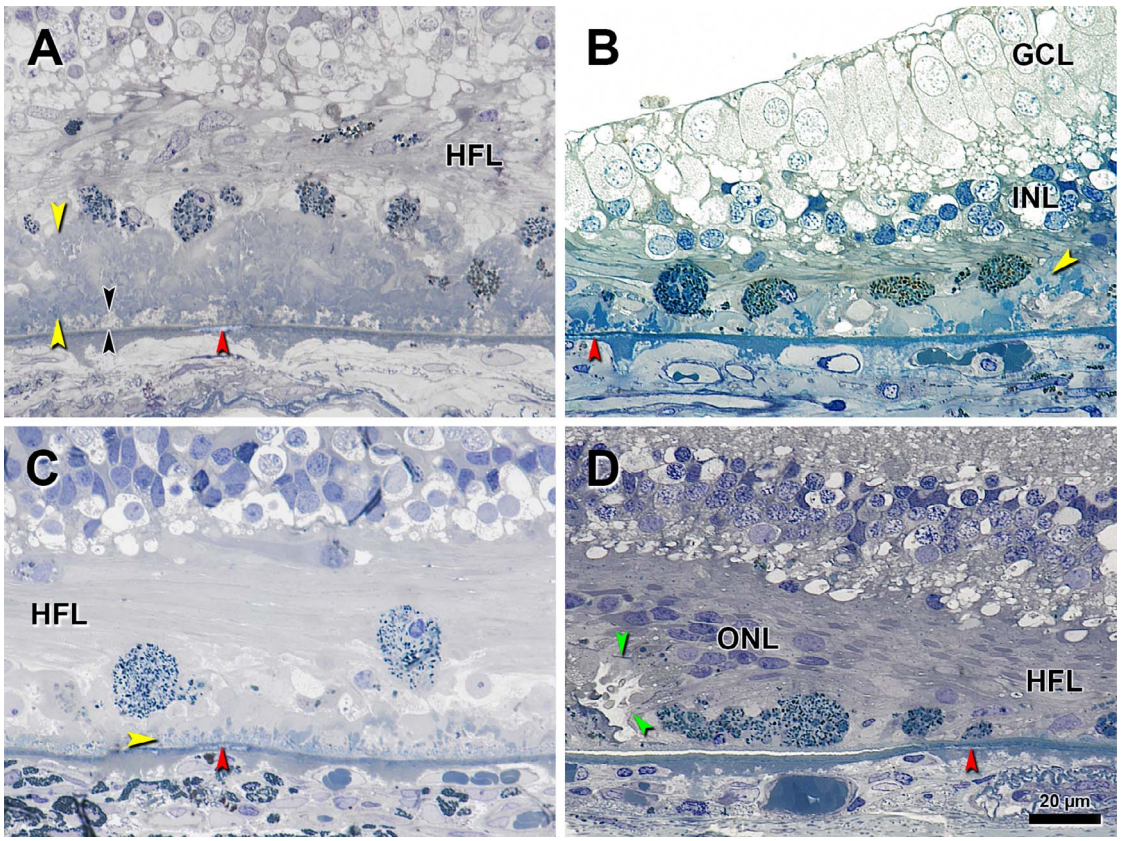

FIGURE 3. 'Dissociated' RPE in eyes with late AMD. *Yellow arrowheads*: BLamD; *red arrowheads*: calcification in BrM; *green arrowheads*: ELM. (**A–C**) Photoreceptors have atrophied, and ELM is absent. (**A**) RPE cells adhere to thick late BLamD. Groups of RPE granules have been shed into BLamD. Isolated granules also spread into HFL. Focal extracellular deposits of gray-stained soft druse material (basal mounds) are visible at outer BLamD (*black arrowheads*). (**B**) 'Dissociated' RPE cells, adherent to BLamD; pigmented granules spread in HFL and in BLamD. (**C**) Two RPE cells detached from BLamD. (**D**) Individual RPE cells on BrM at a GA border with curved ELM and reduced photoreceptor nuclei. GCL, ganglion cell layer; other abbreviations as in Figure 2.

individual granules within retinal layers and granule aggregates within subjacent BLamD (Fig. 3). 'Entombed' RPE is buried by subretinal scars (Figs. 2F, 4); in 213 (71%) locations in CNV eyes, a sub-RPE scar was also present. 'Entombed' RPE cells were rectangular in cross section, not always continuous, often adjacent to cells with insufficient granules to qualify as RPE (Fig. 4A), arranged with similar cells in a double layer (Figs. 4B, 4C), or enveloped by thin basement membrane material. They could also be interposed with extracellular fibrin (Fig. 4C) and extracellular or intracellular fluid (Fig. 4D). Some cells contained spherical as well as spindle-shaped melanosomes.[44]

The distribution of RPE grades by sections and by diagnostic category is presented in Figure 5 and Table 1, and frequencies normalized by total and abnormal grades are presented in Table 2. Because atrophy and scar were mainly centrally located in both GA and CNV eyes, advanced RPE changes were more apparent in Central than Superior sections. In CNV eyes this regional difference was less evident because atrophy was larger. Combining data from Central and Superior sections, 'Atrophy with BLamD' was more frequent than 'Atrophy without BLamD' and overall more abundant in CNV eyes than GA eyes ('with' and 'without': 19.3% and 5.8% for GA; 29.5% and 19.5% for CNV). If the 'Dissociated' grade is pooled with 'Atrophy with BLamD' and 'Atrophy without BLamD,' 'Dissociated' cells were found at 22.2% of all locations with atrophy in GA eyes and at 5.8% of all locations with atrophy in CNV eyes. Considering only abnormal RPE grades (Table 2), we found that 'Shedding' (34.2%), 'Sloughed' (33.3%), and 'Dissociated' (28.1%) were the most prevalent RPE morphologies in GA eyes. 'Entombed' RPE was a major finding in CNV eyes: 37.3% of locations with scar had 'Entombed' RPE (not shown), and 64.3% of all abnormal RPE cells were 'Entombed' (Table 2). If only the six abnormal grades common to both CNV and GA are considered, 'Sloughed' (26.2%), 'Dissociated' (24.4%), and 'Bilaminar' (22.0%) represent the most frequent RPE grades in CNV eyes. The frequency of 'Sloughed' and 'Intraretinal' together was similar in GA and CNV (35.1% and 35.7%, respectively). Yet CNV eyes had far more 'Intraretinal' (9.5%) and fewer 'Sloughed' cells (26.2%) than GA eyes (1.8% and 33.3%, respectively). 'Vacuolated' RPE was uncommon in both GA and CNV (0.9% and 3.0%, respectively).

Figure 6 and Tables 1 and 3 show thicknesses of epithelial RPE and BLamD. Table 3 additionally shows frequency of BLamD occurrence. Mean thickness of 'Nonuniform' RPE was 11.7 ± 2.6 μm in GA eyes and 10.9 ± 2.4 μm in CNV eyes. Of note, RPE thickness did not decrease from 'Nonuniform' RPE through more abnormal RPE grades in either GA or CNV eyes. Thickness of 'Entombed' RPE was almost 1.5-fold higher than that of 'Nonuniform' RPE, because it often contained two layers of similar cells. Relative to 'Nonuniform' RPE, 'Shedding' RPE had 9- to 10-fold thicker BLamD in both GA and CNV eyes, although variability was high. Advanced RPE morphologies were highly associated with BLamD (frequency of occurrence for 'Dissociated,' 97%–100% in GA and CNV; 'Entombed,' 78% in CNV). BLamD persisted in 77% of atrophic locations in GA eyes (mean thickness, 4.7 ± 3.5 μm) and in 60% of atrophic locations in CNV eyes (7.2 ± 6.7 μm).

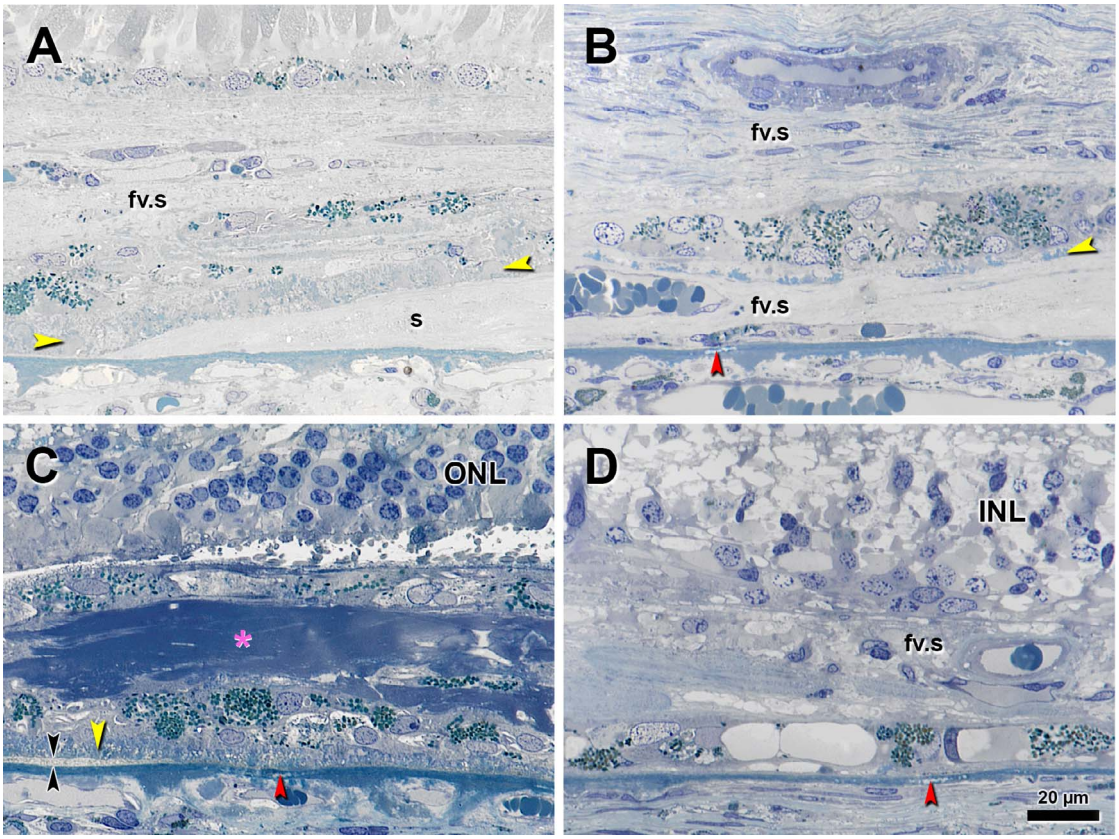

FIGURE 4. 'Entombed' RPE in eyes with CNV. *Yellow arrowheads*: BLamD; *red arrowheads*: calcification in BrM. (**A**) 'Entombed' RPE and nonpigmented cells inside a subretinal fibrovascular scar (fv.s). Thick BLamD separates subretinal fibrovascular scar from sub-RPE fibrous scar (s). A slightly pigmented monolayer on the scar internal aspect contacts photoreceptor inner segments. (**B**) A cluster of cells, with nuclei on two levels, adjacent to thin and discontinuous BLamD is between fibrovascular subretinal and sub-RPE scars (fv.s). (**C**) 'Entombed' RPE intermingled with fibrin (*pink asterisk*). BLinD, *black arrowheads*. Photoreceptor outer and inner segments are lost. (**D**) 'Entombed' RPE cells in a row on BrM inside a fibrovascular subretinal scar (fv.s). The nucleus of RPE cell on the *right* is displaced eccentrically by intracellular fluid. Abbreviations as in Figure 2.

The in vivo visibility of distinctive RPE morphologies by SDOCT imaging was addressed in one case of direct clinicopathologic correlation.[49] The right eye of a 98-year-old white woman with advanced AMD came to histopathology 8 months after multimodal clinical imaging. Because pathology findings were consistent over an extended area and this section matched the corresponding SDOCT scan better than all others, SDOCT correlates for several RPE morphologies were apparent (Fig. 7), even if specific individual cells and granule aggregates could not be linked to specific hyperreflective foci. Figure 7 illustrates imaging–histology correlations for 'Dissociated' cells on BLamD (Figs. 7E–G), 'Dissociated' cells within the INL (Fig. 7F), material shed from 'Shedding' (Fig. 7E), and epithelial and nonepithelial components of 'Sloughed' (Fig. 7G). A fibrovascular scar with hyperreflectivity and possible lamellar substructure is external to a thick and relatively less reflective BLamD. The RPE-BrM band is split by the BLamD-scar combination.[8]

DISCUSSION

In the most extensive survey of RPE morphology in late AMD eyes to date, we capitalized on the ability to distinguish organelles over large tissue expanses, the availability of 52 late AMD eyes, unbiased systematic sampling, and a focus on cardinal features of RPE ultrastructure, particularly spindle-shaped melanosomes. We observed grades seen at lower resolution in smaller series of early and late AMD eyes[31–33,39–43] and defined new RPE grades. Grades were found in both GA and CNV eyes, in different proportions, consistent with a defined repertoire of stress responses accessible by a single histologic grading system. Because contemporary SDOCT provides exquisite structural detail, clinical interpretation is best served by morphological descriptions that are pegged to precise retinal locations, comprehensive, quantitative, and digitally available. From numerous short postmortem eyes, we provided views that were high magnification, high resolution, color, and panoramic, with the original histology accessible online. From the current perspective, we could recognize the same RPE morphologies in previous publications (Table 4). Our clinicopathologic correlation, taken with published histology and clinical imaging (Table 4), suggests that many histologic RPE grades are transferrable to SDOCT.

Our survey, intended primarily as a comprehensive context for clinical imaging, is the first to our knowledge to systematize RPE morphology as hypotheses about major biologic processes testable by future research. These data provide a firm structural basis for future molecular phenotyping. Age-related macular degeneration was advanced in our study eyes, yet data are relevant to questions of pathogenesis. All eyes exhibited areas of early- and intermediate-stage disease outside the main atrophic areas. Further, many morphologies were previously described in early AMD eyes. Finally, the availability of numerous SDOCT volumes of advanced AMD eyes, collected under standardized conditions in clinical trials and in practices with longstanding SDOCT use, means that end stages can be

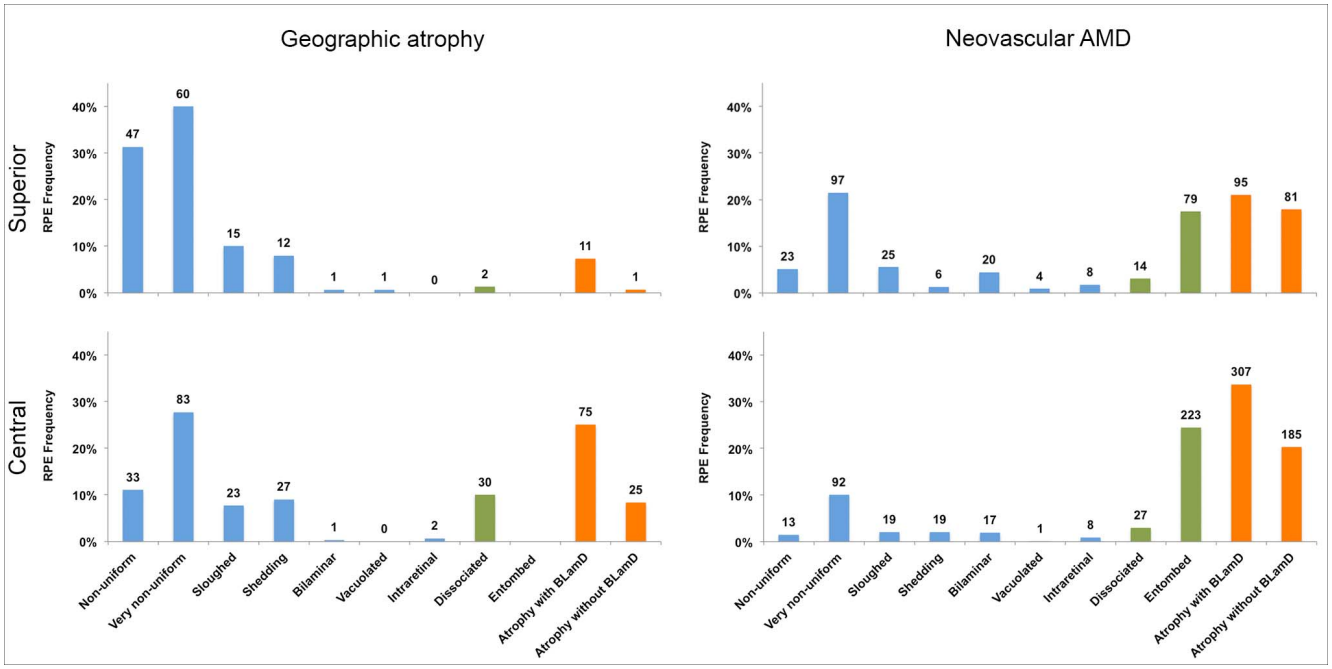

Figure 5. Distribution of RPE grades in eyes with GA and choroidal neovascularization. Superior and Central sections of GA eyes ($n = 13$) and CNV eyes ($n = 39$). The Superior section is located 2 mm superior to the Central section. RPE morphologies are indicated by colored bars: Epithelial (*blue*), Nonepithelial (*green*), and Atrophic (*orange*). The numbers atop each column represent the number of affected locations. RPE morphologies in 150 Superior and 299 Central locations of eyes with GA show many locations with 'Dissociated' and 'Atrophy with BLamD.' RPE morphologies in 452 Superior and 911 Central locations in eyes with CNV show many locations with 'Entombed RPE' and 'Atrophy.'

tracked backward to impart new significance to earlier stages.[50,53–57] Atrophy is absence of a pigmented cell layer that can be explained by death, transdifferentiation to a cell type not meeting our criteria for RPE, or emigration. In Figure 1 and as detailed below, 'Dissociated' and 'Entombed' appear to be final steps before the RPE layer disappears. Only 'Shedding' seems to be actually dying. Some morphologies like 'Sloughing'/'Intraretinal' and others presented in the companion paper[44] suggest transdifferentiation with acquisition of new cellular behaviors. We discuss each RPE phenotype in turn, starting with cells newly described at end-stage AMD.

The definitions of GA in color fundus photography, SDOCT, and fundus autofluorescence[58–60] all imply absence of differentiated RPE, yet within the atrophic zone we found many granule-rich 'Dissociated' RPE cells, usually accompanied by BLamD. Of atrophic locations in GA eyes, a sizeable minority (22.2%) had 'Dissociated' RPE, 4-fold higher than in CNV eyes. 'Dissociated' cells are a likely source of cellular fragments and single granules, particularly in the Henle fiber layer, that manifest as autofluorescent debris.[33] The most plausible predecessors of 'Dissociated' RPE are the epithelial components of 'Sloughed'/'Intraretinal' and 'Shedding' (Fig. 1), which like 'Dissociated' sit atop BLamD and could eventually break up as cells or fragments exit the layer (see below). Clinical SDOCT observations (Table 4) of an elevated RPE-BrM band manifesting as a hyperreflective "dotted line throughout the atro-

Table 2. Percentages of RPE Phenotypes Referenced to Total and Abnormal* Morphologies

	Geographic Atrophy, Superior + Central		Choroidal Neovascularization, Superior + Central		
	RPE Grade %		RPE Grade %		
RPE Grade	Referenced to Total, $N = 449$	Referenced to 6 Grades, $N = 114$	Referenced to Total, $N = 1363$	Referenced to 6 Grades, $N = 168$	Referenced to 6 Grades + Entombed, $N = 470$
'Sloughed'	8.5	33.3	3.2	26.2	9.4
'Shedding'	8.7	34.2	1.8	14.9	5.3
'Bilaminar'	0.4	1.8	2.7	22.0	7.9
'Vacuolated'	0.2	0.9	0.4	3.0	1.1
'Intraretinal'	0.4	1.8	1.2	9.5	3.4
'Dissociated'	7.1	28.1	3.0	24.4	8.7
'Entombed'	n.a.	n.a.	22.2		64.3

n.a., not available; 'Entombed' RPE are found in neovascular AMD eyes only.

* Mechanistically heterogeneous category includes RPE cells thought to be degenerating ('Shedding'), nonepithelial ('Dissociated' and 'Entombed'), and transdifferentiating (nonepithelial) components of 'Sloughed'/'Intraretinal,' which appear to be migratory, and others for which mechanisms and functional significance are currently unknown ('Bilaminar,' 'Vacuolated').

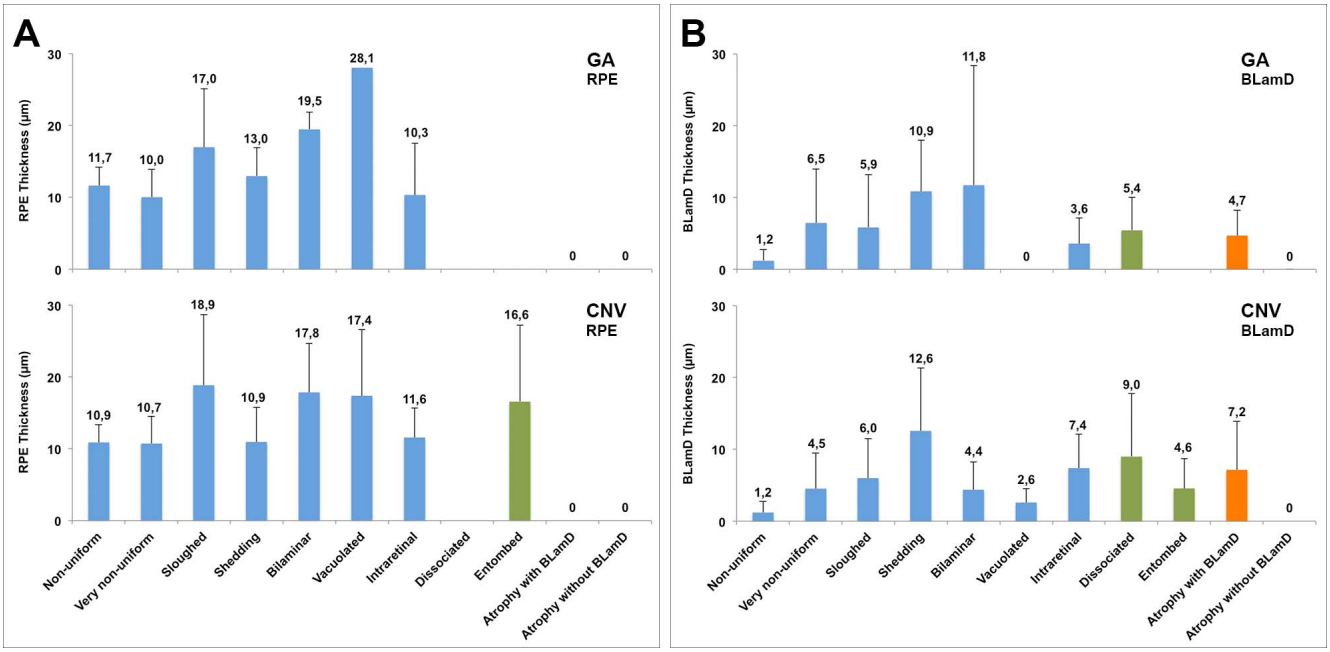

Figure 6. RPE and BLamD thickness in eyes with advanced AMD. Epithelial, Nonepithelial, and Atrophic RPE are *blue*, *green*, and *orange bars*, respectively. At the *top of each column* is mean RPE or BLamD thickness in combined Superior and Central sections. Same sample size as in Figure 5. (**A**) RPE thickness does not decrease with perturbed morphology. Trends for different RPE morphologies are similar between GA and CNV eyes. 'Entombed' RPE's thickness is >1.5 times that of Nonuniform RPE. (**B**) BLamD thickness is maintained with advancing pathology.

phy"[59(p4140)] and dots on BrM itself[61] are consistent with 'Dissociated' cells. Direct evidence of a transition between 'Sloughed' and 'Dissociated' is revealed by SDOCT imaging over 13 months in a "diffuse trickling" (multilobular) GA eye (Fig. 6[62]; Fleckenstein M, written communication, 2014).Our observations confirm and extend histologic illustrations[29] and descriptions of "melanin dispersion inside areas of GA" by Gocho et al[17(p3670)] revealed by adaptive optics assisted near-infrared reflectance imaging.[17] Also seen with this technology were clumps, 30 to 40 µm in diameter, apparently motile on a time course of weeks. These were attributed to extracellular or intracellular melanosomes (within dysmorphic RPE, Müller cells, macrophages, or microglia).[17] 'Dissociated' RPE is the leading histologic correlate for this remarkable phenomenon.

Illustrated in previous histology, 'Entombed' RPE appears at 37.3% of locations with fibrovascular and fibrocellular scar (Table 4). Originally called entrapped,[63] these cells are herein named 'Entombed' in distinction to entrapment sites (incipient drusen) on inner BrM.[64] 'Entombed' RPE, frequently a double layer, may signify RPE folding back on itself as CNV breaks through to the subretinal space,[65] so that apical surfaces appose,[66] or RPE tears as the scar contracts,[67,68] so that basal surfaces also might appose. Although SDOCT can disclose abundant detail in subretinal fibrovascular material,[69] signatures consistent with 'Entombed' RPE remain to be defined. Polarization-sensitive OCT, however, reveals a discontinuous line of residual polarization scramblers in these locations (Table 4). 'Entombed' RPE expresses RPE markers[70] and, consistent with its granule population, exhibits histologic autofluorescence[71] and thus possibly fundus autofluorescence signal as well. Our companion paper shows evidence for transdifferentiation of 'Entombed' to 'Melanotic' cells.[44] Functional capacities, life cycle, and role of 'Entombed' RPE in antivascular endothelial growth factor therapy, if any, remain to be learned.

Table 3. Thicknesses of RPE and Thicknesses and Frequencies of BLamD, by RPE grade in GA and CNV Eyes

	Geographic Atrophy, Superior + Central		Choroidal Neovascularization, Superior + Central	
RPE Grade	Locations With BLamD, No./Total at Grade, %	Mean Thickness, µm	Locations With BLamD, No./Total at Grade, %	Mean Thickness, µm
'Nonuniform'	40/80, 50	1.2 ± 1.5	16/36, 44	1.2 ± 1.5
'Very Nonuniform'	127/143, 89	6.5 ± 7.5	138/189, 73	4.5 ± 4.9
'Sloughed'	33/38, 87	5.9 ± 7.3	37/44, 84	6.0 ± 4.5
'Shedding'	39/39, 100	10.9 ± 7.2	25/25, 100	12.6 ± 8.7
'Bilaminar'	1/2, 50	11.8 ± 16.6	29/37, 78	4.4 ± 3.9
'Vacuolated'	0/1, 0	0	4/5, 80	2.6 ± 1.9
'Intraretinal'	2/2, 100	3.6 ± 3.5	15/16, 94	7.4 ± 4.7
'Dissociated'	31/32, 97	5.4 ± 4.6	41/41, 100	9.0 ± 8.8
'Entombed'	n.a.	n.a.	235/302, 78	4.6 ± 4.2
'Atrophy with BLamD'	86/86, 100	4.7 ± 3.5	402/402, 100	7.2 ± 6.7
'Atrophy without BLamD'	0/26, 0	0	0/266, 0	0

n.a., not available; 'Entombed' RPE are found in neovascular AMD eyes only.

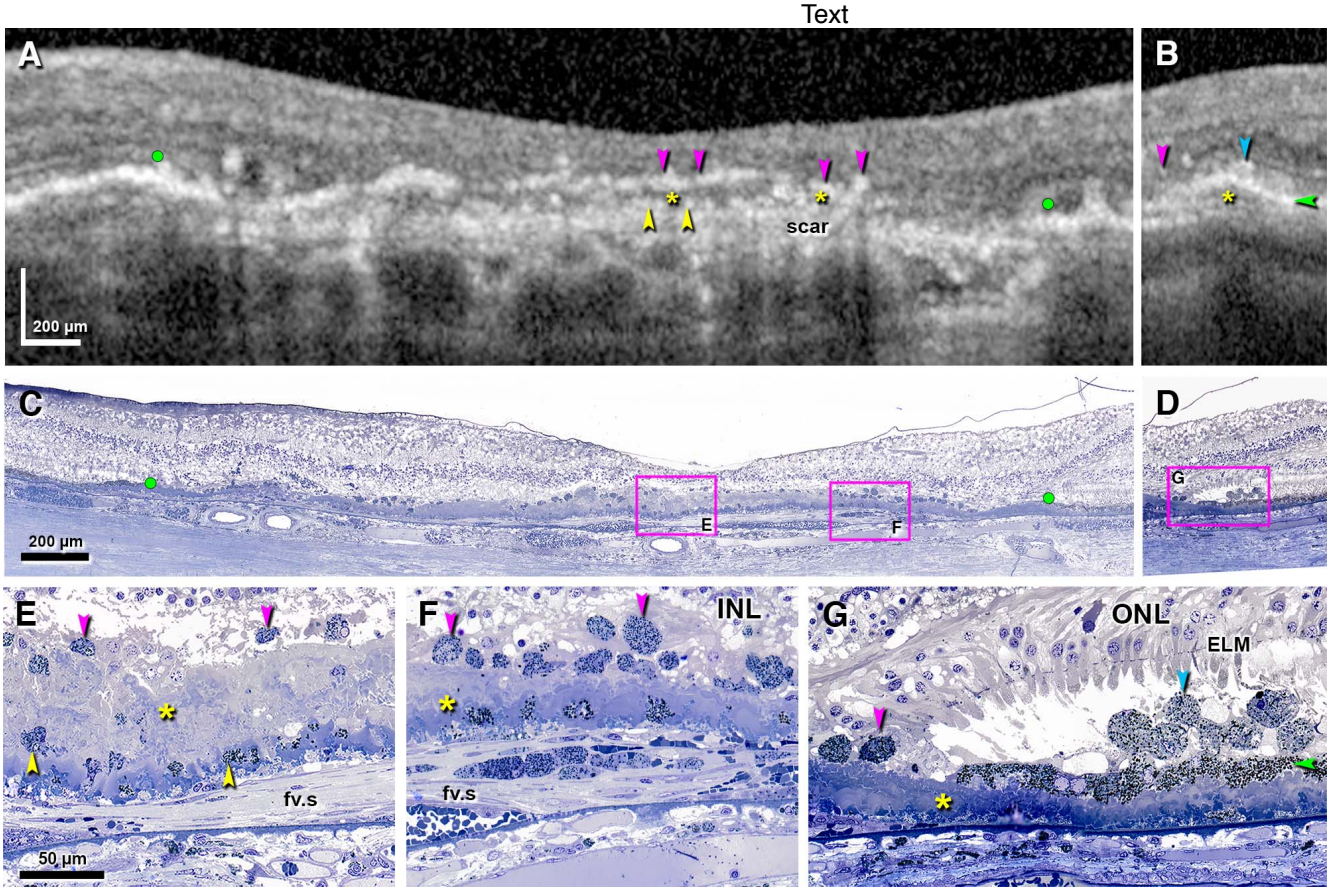

Figure 7. Clinicopathologic correlation of RPE morphologies. The right eye of a 98-year-old white woman with advanced AMD (both GA and CNV) was clinically examined with SDOCT imaging 8 months before death. (**A**, **B**) In vivo SDOCT scans match histology (**C**, **D**), respectively. GA borders are defined by the end of curved ELM (*green dots*) in (**A**, **C**). *Bar* in (**A**) applies to both. (**A**) Increased choroidal reflectivity in GA and hyperreflective scar over BrM. A dotted hyperreflective line crosses GA (*pink arrowheads*). It is separated from the scar by a hyporeflective layer (*yellow asterisk*) containing additional hyperreflective dots (*yellow arrowhead*). (**B**) Hyperreflective dots (*blue arrowhead*) over a continuous RPE-BrM complex band (*green arrowhead*) outside GA and individual hyperreflective dots inside GA (*pink arrowhead*). The ELM band is visible. (**C**, **D**) Low magnification of different histologic sections from this eye that match SDOCT scans in (**A**, **B**). *Bar* in (**C**) applies to both. (**C**) Central GA and sub-RPE fibrovascular scar. Multiple Dissociated RPE cells overlie very thick BLamD containing granule aggregates (**E**, **F**). Inner retinal layers are continuous outside the gap at the foveal depression. (**D**) GA border; 'Nonuniform' and 'Sloughed' RPE outside GA, two 'Dissociated' RPE cells inside GA. (**E**–**G**) High magnification of histology of (**A**, **B**). BLamD, *yellow asterisk*; fv.s, fibrovascular scar. *Bar* in (**E**) applies to all. It was possible to match classes of hyperreflective spots to classes of cells, if not individual cells and spots. However, the configurations of spots in (**A**) and cells in (**E**–**G**) are not identical. (**E**) 'Dissociated' nucleated RPE cells (*pink arrowhead*) on thick early and late BLamD with granule aggregates and two granule-containing cells (a rare finding, *yellow arrowhead*). (**F**) 'Dissociated' RPE cells (*pink arrowhead*) lying on BLamD and 'Dissociated' RPE cells migrating toward the INL. 'Shedding' RPE inside BLamD (*yellow arrowhead*). With ELM absent, these cells are not called 'Intraretinal.' Pigmented cells located within the scar are 'Subducted'[44]; their reflectivity may be indistinguishable from that of the surrounding scar. (**G**) Epithelial (*green arrowhead*) and nonepithelial (*blue arrowhead*) cells of the 'Sloughed' morphology, in the subretinal space outside GA. Two 'Dissociated' RPE cells are seen inside GA (*pink arrowhead*).

Previously described[32,33] 'Sloughed' and 'Intraretinal' morphologies appear to be two phases of a continuum featuring nonepithelial cells internal to an epithelial layer that then apparently disintegrates (see above). Because we found in the subretinal space almost exclusively fully pigmented cells, and because 'Sloughed'/'Intraretinal' cells were packed with RPE granules of morphology and packing density similar to subjacent epithelial RPE, we considered them RPE derived. The identity of pigmented cells in the subretinal space has been debated for decades, with the two leading contenders RPE and monocyte-derived macrophages/microglia that phagocytized RPE and retained telltale melanosomes.[17,72–74] Investigators using single-section TEM to visualize these cells in experimental thermal injury and retinal detachment considered them RPE derived because of numerous intracellular granules nondelimited by a phagosome membrane, abundant smooth endoplasmic reticulum, and loss of apical microvilli and junctional complexes in transitioning to nonepithelial.[75–78] Recent evidence indicates that numerous Iba-1-immunoreactive microglia reside in the subretinal space of aged mice[79–85] and appear also in human retinal degenerations including AMD.[79,86,87] Our technique was not optimized for detecting widely scattered, small-body microglia, although we certainly sought such cells, as they can be recognized without selective labels.[88] 'Sloughed' RPE has been pictured and described in mouse models of iron overload and mitochondrial dysregulation,[89,90] consistent with a stereotypic response repertoire. 'Intraretinal' RPE was not reported, however, suggesting that signals prompting inward migration (e.g., vitreous factors[91–94]) and coordinated opening of the ELM remain to be determined. Interestingly, in a mouse with RPE-specific expression of Cre, subretinal melanosome-bearing cells were Cre-immunoreactive and considered definitive RPE origin; the same study also showed a macrophage marker in 2% of epithelial RPE.[90] We hypothesize that 'Sloughed'/'Intraretinal' cells are RPE originated and transdifferentiate to a migratory and possibly

Table 4. Previous Literature Showing RPE Morphologies

Morphology	Histology References	SDOCT References
'Nonuniform'	Fig. 4[33]	*
'Very Nonuniform'	Figs. 4I, 4B[63]; Fig. 17[29]; Figs. 9, 22[130]; Fig. 2[131]; Fig. 24[132]; Figs. 3, 5[43]	Fig. 5A[133]
'Sloughed'	Figs. 3, 8[39]; Figs. 5, 9[134]; Figs. 12, 16[29]; Fig. 6[135]; Fig. 2[42]; Figs. 1D, 3A, 4D[71]; Fig. 1[31]; Fig. 9[136]; Fig. 3[32]; Fig. 5[33]; Fig. 14[137]	Fig. 4I[138]; Fig. 6[62]; Fig. 2[126]
'Shedding'	Fig. 12[29]; Figs. 1, 2[31]; Fig. 3[32]; Fig. 5[33]	Figs. 4I, 5D, 5F[138]
'Bilaminar'	Figs. 2B, 4 (TEM)[66]; Fig. 20[29]; Figs. 2, 11[65]; Fig. 5[131]; Fig. 3[32]; Fig. 5[33]	†
'Vacuolated'	‡	§
'Intraretinal'	Figs. 2, 4[42]	Fig. 4I[138]; Figs. 4, 6[139]; Figs. 4, 5[140]
'Dissociated'	Figs. 20, 26[29]; Fig. 8[17]	On BLamD: Figs. 5F, 6B, 7E[138]; Fig. 5[141]; Figs. 3C, 6A[133]; Fig. 6[62]; Fig. 3[142]; on BrM: Figs. 4K, 4L[61]
'Entombed'	Figs. 4I, 50A[63]; Fig. 6[66]; Fig. 18[48]; Fig. 9[70]; Fig. 5[143]; Figs. 1, 4[144]; Fig. 20[130]; Fig. 13[131]; Figs. 2, 3, 13[145]; Fig. 7[146]; Figs. 4B, 4C[71]; Fig. 25[132]; Figs. 2, 11[113]	Fig. 8[61]; Fig. 8[139]
'Atrophy with BLamD'	Fig. 45[63]; Fig. 2[146]	Figs. 7C, 7F, 7G[138]; Fig. 2[53]; Fig. 2[8]
'Atrophy without BLamD'	||	Fig. 7A[138]; Fig. 6B[133]

Published images were assigned to specific grades by authors ECZ and CAC using the grading system in the current paper.
* Not usually specified.
† Not identified yet.
‡ Previously seen only in mice; see text.
§ Not identified yet.
|| No interpretable images.

phagocytic phenotype, and that in addition to retaining abundant melanosomes they express markers consistent with newly acquired behaviors. The current data cannot conclusively distinguish between RPE transdifferentiation in this manner and an invasion of phagocytes, although we suggest that the latter would contain variable granule composition and concentration reflecting variable times post phagocytosis. Quantitative comparison of multiple markers and ultrastructural features in a statistically robust sample of 'Sloughed'/'Intraretinal' cells, epithelial RPE, and monocytes is needed to resolve these questions; such studies are planned.

'Sloughed' and 'Intraretinal' morphologies are excellent candidates for the subretinal and intraretinal hyperreflective foci repeatedly observed on SDOCT (Table 4) and interpreted variably as "dead RPE and melanin-containing macrophages,"[59] "activated RPE cells,"[95] and "inflammatory cells (e.g., retinal microglia)."[74] Multimodal clinical imaging reveals the dynamism and prognostic importance of these cells. Hyperreflective spots are related to hyperpigmentation revealed by color photography[74,96]; they migrate into inner retinal layers,[59,95] and their quantity and density increase first perifoveally and then foveally in a 2-year period marked by GA incidence.[95] Of interest was the high proportion of 'Intraretinal' cells in CNV eyes relative to GA eyes, due to either factors promoting intraretinal migration or additional cellular sources beyond 'Sloughed.' The basis of intraretinal hyperreflective foci in late AMD is multifactorial, and determining what cells contribute is an important research goal.

'Shedding' RPE was first proposed as a major RPE progression pathway by our group,[32,33] and these and separately reported data[52] suggest that 'Shedding' is undergoing cellular fragmentation. The basolaterally shed granules usually do not scatter, suggesting that cohesion is actively maintained, perhaps with an enclosing cytosol gel. In separate studies, we will show that RPE lipofuscin redistributes intracellularly in AMD by forming aggregations 2 to 20 μm in diameter containing autofluorescent LF/MLF surrounded by cytoplasm, events more readily seen in en face flat mounts than in cross-sectional histology.[52] These intracellular aggregates are credible forerunners of the aggregates released into BLamD. Our observations do not contradict those of Burns and Feeney-Burns,[97] who showed RPE cytoplasm lacking lipofuscin shed into small drusen without BLamD. Seminal ultrastructural studies described apoptotic bodies in cells fated for regulated cell death as membrane-delimited inclusions condensed by extrusion of water, sometimes containing nuclear chromatin but largely reflecting composition of the local cytoplasm.[98] Given the huge number of LF/MLF granules in aged human RPE,[52] it is not surprising that apoptotic bodies could be concentrations of these organelles. In FAS ligand (tumor necrosis superfamily member 6)-triggered apoptosis, activated caspases-8 and -3 are widely considered initiator and executor mechanisms,[99] respectively, and the RPE layer in GA exhibits immunoreactivity for both.[100,101] If these proteins should localize to specific cellular phenotypes, then it may be possible to monitor apoptosis and the effect of cytoprotective agents in vivo via the SDOCT signal of shed granule aggregates. Our direct clinicopathologic correlation and published SDOCT images of the GA junctional zone (Table 4) illustrate hyperreflective dots within thick BLamD,[8] enhancing the prospects of in vivo monitoring. The 'Shedding' phenotype may appear in the apoE4 transgenic mouse[102] yet has not appeared in other mouse strains with thick BLamD.[103–105]

Several minority RPE morphologies await further exploration. First described by our group in GA,[32,33] 'Bilaminar' RPE exhibit superimposed cytoskeletal arrays (Supplementary Fig. S2). Limited data suggest that the outer layer may be partly dedifferentiated with regard to protein expression.[32] Like 'Entombed' RPE, also often double-layered, 'Bilaminar' RPE was found more frequently in eyes with CNV than in GA eyes, suggesting a relationship. Yet we did not observe interpretable transitions between 'Bilaminar' and 'Entombed,' perhaps due to the timing of our observations relative to CNV initiation. Another minority morphology was 'Vacuolated,' previously reported over small drusen[106] and in mouse models exhibiting vacuoles either within the RPE monolayer[88,102,107] or intruding

into the layer of outer segments.[84,88,108] Separately we describe in AMD eyes mushroom-shaped cells with a stem in the RPE layer and a cap of autofluorescent lipofuscin granules extending into the layer of outer segments.[52] These rare cells may or may not correspond to 'Vacuolated' RPE. More data are needed to deconstruct the heterogeneous 'Vacuolated' category, to determine if they are truly rare or just a transient phase, and to identify in vivo imaging correlates.

In quantifying RPE thickness in AMD systematically for the first time, we found that the RPE layer became highly variable and overall thicker as cells became less epithelial in both GA and CNV eyes, despite small numbers at some grades. Our mean thickness for 'Nonuniform' RPE was 11.7 ± 2.6 μm and 10.9 ± 2.4 μm in GA and CNV eyes, respectively, agreeing with 11.3 ± 1.4 μm reported by Spraul et al.[41] and thinner than normal aged eyes.[109] The compact shape of healthy RPE is energetically efficient, and individual cells thin as the RPE layer effaces over apices of hard drusen.[97,110] Existing histopathology[33,111] shows maintained or increased RPE thickness at the GA border, contrary to a recent SDOCT interpretation.[112] The large size of nonepithelial cells pertains to whether these cells are hyperplastic (i.e., proliferating) or hypertrophic.[113] We favor hypertrophy, as we utilized fine detail of nuclear chromatin to focus images, and no mitotic figures were encountered, suggesting that any cell division occurs rarely. Further, the nonepithelial component of 'Intraretinal' appeared larger (i.e., hypertrophic) than its epithelial counterparts (Fig. 2E). Because larger cells are encountered more frequently than smaller cells in a given histologic section, they could be perceived as proliferating. Finally, RPE layer thickening with disease severity can help explain the poor and even negative predictive value of fundus hyperautofluorescence for progression at a cellular level at GA borders,[114,115] where cells are thick or stacked.[33] A thicker layer represents a greater workload for cells with clearance capacity like Müller cells or microglia, thus delaying the onset of atrophy.

BLamD thickness is maintained even as the RPE degenerates. BLamD forms small pockets between the RPE and its basal lamina in many older normal eyes, and a continuous layer in AMD eyes.[9,39,116,117] BLamD is a frequently overlooked portion of AMD pathology[118,119] despite being a marker of progression risk and RPE stress.[39] We propose that thick BLamD constitutes a fourth form of RPE detachment, along with drusenoid, serous, and fibrovascular. We found that in CNV eyes, BLamD associated with 'Dissociated' RPE was thicker than that associated with 'Entombed' RPE (Fig. 6), suggesting that 'Dissociated' RPE, replete with RPE granules although degenerating, are more capable of maintaining BLamD than 'Entombed' RPE, with fewer granules. Thick, intrinsically autofluorescent BLamD[120] could account for atrophy appearing homogeneously gray rather than black in autofluorescence imaging of rapidly progressing GA.[62,121,122] It is further possible that 'Dissociated' RPE will be detectable as punctate hyperautofluorescent foci on that background.

In conclusion, our survey of RPE morphology is analogous to reconstructing evolution from the fossil record and should be viewed in light of limitations. These include definitions restricted to perikaryal morphology due to the delicacy of apical processes,[123] limited clinical histories, nongeneralizability to the overall population due to the choice of eyes and sampling methods, and lack of molecular phenotyping due to glutaraldehyde fixation (which is perhaps addressable[124]). Further, the 'Nonuniform' category likely includes subcategories that will be better defined in en face view.[52] Nevertheless, by providing RPE visualization targets to inform image interpretation and instrumentation design, we empower the testing of our overall hypothesis (Fig. 1) in large populations of longitudinally imaged patients.[56,125–127] Knowledge of temporal relationships and clinical outcomes will clarify whether the proposed phenotypes represent harmful or beneficial cellular responses and whether as anatomical biomarkers they provide prognostic value. In the near term, by demonstrating the extent of RPE responses to microenvironmental stressors, we provide readouts and quantitative benchmarks for eliciting similar responses in experimental systems, as well as motivation for high-resolution immunohistochemistry of appropriately preserved new tissues. Animal models of the 'Sloughed'/'Intraretinal' and 'Shedding' phenotypes should prove highly informative. Further, as cytoprotective or trophic RPE support is contemplated for AMD,[128,129] multiple stress responses strongly motivate better understanding of the complex microenvironments that will be encountered by these cells. Finally, by indicating how many cells along different pathways may be responsive to specific interventions, our data can inform therapeutic strategies.

Acknowledgments

We thank personnel of the Alabama Eye Bank (Doyce V. Williams, CEBT, CBTS, executive director, and Alan S. Blake, CEBT, CBTS, chief technical officer) for timely retrieval of donor eyes; personnel of the Eye Bank for Sight Restoration (Patricia Dahl, CEBT, executive director, New York) for recovering tissue from a clinically documented donor; donor families for their generosity; Nancy E. Medeiros, MD, for assistance in evaluating ophthalmic histories of eye donors; Kristen Hammack, BS, for ImageJ support; and Giovanni Staurenghi, MD, for facilitating the participation of author ECZ.

Supported by National Eye Institute (NEI) R01 EY06109 with institutional support from the EyeSight Foundation of Alabama and Research to Prevent Blindness, Inc. (CAC, JDM); University of Milan and NEI R01 EY015520 (ECZ); DFG (German Research Foundation) AC265/1-1 and AC265/2-1 (TA) and NEI R01 EY015520 (RTS); NEI R01 EY 021470 and EY 015520 (RTS); and the Macula Foundation (KBF). Acquisition of donor eyes was additionally supported by the International Retinal Research Foundation, NEI P30 EY003039, and the Arnold and Mabel Beckman Initiative for Macular Research. Creation of Project MACULA was additionally supported from the Edward N. and Della L. Thome Memorial Foundation.

Disclosure: **E.C. Zanzottera**, None; **J.D. Messinger**, None; **T. Ach**, None; **R.T. Smith**, None; **K.B. Freund**, None; **C.A. Curcio**, None

References

1. Klaver CC, Wolfs RC, Vingerling JR, Hofman A, de Jong PT. Age-specific prevalence and causes of blindness and visual impairment in an older population: the Rotterdam Study. *Arch Ophthalmol*. 1998;116:653–658.
2. Day S, Acquah K, Lee PP, Mruthyunjaya P, Sloan FA. Medicare costs for neovascular age-related macular degeneration, 1994-2007. *Am J Ophthalmol*. 2011;152:1014–1020.
3. Verbrugge L, Patrick D. Seven chronic conditions: their impact on U. S. adults' activity levels and use of medical services. *Am J Public Health*. 1995;85:173–182.
4. Fritsche LG, Fariss RN, Stambolian D, Abecasis G, Curcio CA, Swaroop A. Age-related macular degeneration: genetics and biology coming together. *Annu Rev Genomics Hum Genet*. 2014;15:151–171.
5. Shi G, Maminishkis A, Banzon T, et al. Control of chemokine gradients by the retinal pigment epithelium. *Invest Ophthalmol Vis Sci*. 2008;49:4620–4630.
6. Curcio CA. Complementing apolipoprotein secretion by retinal pigment epithelium. *Proc Natl Acad Sci U S A*. 2011;108:18569–18570.

7. Booij JC, ten Brink JB, Swagemakers SM, et al. A new strategy to identify and annotate human RPE-specific gene expression. *PLoS One*. 2010;5:e9341.
8. Ooto S, Vongkulsiri S, Sato T, Suzuki M, Curcio CA, Spaide RF. Outer retinal corrugations in age-related macular degeneration. *JAMA Ophthalmol*. 2014;132:806–813.
9. Sarks S, Cherepanoff S, Killingsworth M, Sarks J. Relationship of basal laminar deposit and membranous debris to the clinical presentation of early age-related macular degeneration. *Invest Ophthalmol Vis Sci*. 2007;48:968–977.
10. Johnson LV, Forest DL, Banna CD, et al. Cell culture model that mimics drusen formation and triggers complement activation associated with age-related macular degeneration. *Proc Natl Acad Sci U S A*. 2011;108:18277–18282.
11. Klein ML, Ferris FL III, Armstrong J, et al. Retinal precursors and the development of geographic atrophy in age-related macular degeneration. *Ophthalmology*. 2008;115:1026–1031.
12. Ferris FL III, Wilkinson CP, Bird A, et al. Clinical classification of age-related macular degeneration. *Ophthalmology*. 2013;120:844–851.
13. Zarbin MA, Casaroli-Marano RP, Rosenfeld PJ. Age-related macular degeneration: clinical findings, histopathology and imaging techniques. *Dev Ophthalmol*. 2014;53:1–32.
14. Delori F, Greenberg JP, Woods RL, et al. Quantitative measurements of autofluorescence with the scanning laser ophthalmoscope. *Invest Ophthalmol Vis Sci*. 2011;52:9379–9390.
15. Scoles D, Sulai YN, Dubra A. In vivo dark-field imaging of the retinal pigment epithelium cell mosaic. *Biomed Opt Express*. 2013;4:1710–1723.
16. Rossi EA, Rangel-Fonseca P, Parkins K, et al. Imaging of retinal pigment epithelium cells in age related macular degeneration. *Biomed Opt Express*. 2013;4:2527–2539.
17. Gocho K, Sarda V, Falah S, et al. Adaptive optics imaging of geographic atrophy. *Invest Ophthalmol Vis Sci*. 2013;54:3673–3680.
18. Palczewska G, Dong Z, Golczak M, et al. Noninvasive two-photon microscopy imaging of mouse retina and retinal pigment epithelium through the pupil of the eye. *Nat Med*. 2014;20:785–789.
19. Smith RT, Post R, Johri A, et al. Simultaneous decomposition of multiple hyperspectral datasets: fluorophore signal recovery in the retinal pigment epithelium (RPE). *Biomed Opt Express*. 2014;5:4171–4185.
20. Spaide RF, Curcio CA. Drusen characterization with multimodal imaging. *Retina*. 2010;30:1441–1454.
21. Pircher M, Hitzenberger CK, Schmidt-Erfurth U. Polarization sensitive optical coherence tomography in the human eye. *Prog Retin Eye Res*. 2011;30:431–451.
22. Keane PA, Heussen FM, Ouyang Y, et al. Assessment of differential pharmacodynamic effects using optical coherence tomography in neovascular age-related macular degeneration. *Invest Ophthalmol Vis Sci*. 2012;53:1152–1161.
23. Orlow SJ. Melanosomes are specialized members of the lysosomal lineage of organelles. *J Invest Dermatol*. 1995;105:3–7.
24. Schraermeyer U, Heimann K. Current understanding on the role of retinal pigment epithelium and its pigmentation. *Pigment Cell Res*. 1999;12:219–236.
25. Dell'Angelica EC, Mullins C, Caplan S, Bonifacino JS. Lysosome-related organelles. *FASEB J*. 2000;14:1265–1278.
26. Zhang QX, Lu RW, Messinger JD, Curcio CA, Guarcello V, Yao XC. In vivo optical coherence tomography of light-driven melanosome translocation in retinal pigment epithelium. *Sci Rep*. 2013;3:2644.
27. Wilson JD, Foster TH. Characterization of lysosomal contribution to whole-cell light scattering by organelle ablation. *J Biomed Opt*. 2007;12:030503.
28. Feeney-Burns L, Hilderbrand E, Eldridge S. Aging human RPE: morphometric analysis of macular, equatorial, and peripheral cells. *Invest Ophthalmol Vis Sci*. 1984;25:195–200.
29. Sarks JP, Sarks SH, Killingsworth MC. Evolution of geographic atrophy of the retinal pigment epithelium. *Eye*. 1988;2:552–577.
30. Feher J, Kovacs I, Artico M, Cavallotti C, Papale A, Balacco Gabrieli C. Mitochondrial alterations of retinal pigment epithelium in age-related macular degeneration. *Neurobiol Aging*. 2006;27:983–993.
31. Guidry C, Medeiros NE, Curcio CA. Phenotypic variation of retinal pigment epithelium in age-related macular degeneration. *Invest Ophthalmol Vis Sci*. 2002;43:267–273.
32. Vogt SD, Curcio CA, Wang L, et al. Retinal pigment epithelial expression of complement regulator CD46 is altered early in the course of geographic atrophy. *Exp Eye Res*. 2011;93:413–423.
33. Rudolf M, Vogt SD, Curcio CA, et al. Histologic basis of variations in retinal pigment epithelium autofluorescence in eyes with geographic atrophy. *Ophthalmology*. 2013;120:821–828.
34. Eagle RC Jr, Lucier AC, Bernardino VB Jr, Yanoff M. Retinal pigment epithelial abnormalities in fundus flavimaculatus: a light and electron microscopic study. *Ophthalmology*. 1980;87:1189–1200.
35. McDonnell PJ, Kivlin JD, Maumenee IH, Green WR. Fundus flavimaculatus without maculopathy. A clinicopathologic study. *Ophthalmology*. 1986;93:116–119.
36. Steinmetz RL, Garner A, Maguire JI, Bird AC. Histopathology of incipient fundus flavimaculatus. *Ophthalmology*. 1991;98:953–956.
37. Birnbach CD, Järveläinen M, Possin DE, Milam AH. Histopathology and immunocytochemistry of the neurosensory retina in fundus flavimaculatus. *Ophthalmology*. 1994;101:1211–1219.
38. Bonilha VL, Rayborn ME, Bell BA, Marino MJ, Fishman GA, Hollyfield JG. Retinal histopathology in eyes from a patient with Stargardt disease caused by compound heterozygous ABCA4 mutations. *Ophthalmic Genet*. 2014;1–11.
39. Sarks SH. Ageing and degeneration in the macular region: a clinico-pathological study. *Br J Ophthalmol*. 1976;60:324–341.
40. van der Schaft TL, Mooy CM, de Bruijn WC, Oron FG, Mulder PGH, de Jong PTVM. Histologic features of the early stages of age-related macular degeneration. *Ophthalmology*. 1992;99:278–286.
41. Spraul CW, Lang GE, Grossniklaus HE. Morphometric analysis of the choroid, Bruch's membrane, and retinal pigment epithelium in eyes with age-related macular degeneration. *Invest Ophthalmol Vis Sci*. 1996;37:2724–2735.
42. Curcio CA, Medeiros NE, Millican CL. The Alabama age-related macular degeneration grading system for donor eyes. *Invest Ophthalmol Vis Sci*. 1998;39:1085–1096.
43. Curcio CA, Messinger JD, Sloan KR, McGwin G Jr, Medeiros NE, Spaide RF. Subretinal drusenoid deposits in non-neovascular age-related macular degeneration: morphology, prevalence, topography, and biogenesis model. *Retina*. 2013;33:265–276.
44. Zanzottera EC, Messinger JD, Ach T, Smith RT, Curcio CA. Subducted and melanotic cells in advanced age-related macular degeneration are derived from retinal pigment epithelium. *Invest Ophthalmol Vis Sci*. 2015;56:3269–3278.
45. Schaal KB, Freund KB, Litts KM, Zhang Y, Messinger JD, Curcio CA. Outer retinal tubulation in age-related macular degeneration: optical coherence tomographic findings correspond with histology. *Retina*. In press.
46. Curcio CA, Saunders PL, Younger PW, Malek G. Peripapillary chorioretinal atrophy: Bruch's membrane changes and photoreceptor loss. *Ophthalmology*. 2000;107:334–343.

Investigative Ophthalmology & Visual Science

47. Biesemeier A, Taubitz T, Julien S, Yoeruek E, Schraermeyer U. Choriocapillaris breakdown precedes retinal degeneration in age-related macular degeneration. *Neurobiol Aging*. 2014;35: 2562–2573.
48. Green WR, Enger C. Age-related macular degeneration histopathologic studies: the 1992 Lorenz E. Zimmerman Lecture. *Ophthalmology*. 1993;100:1519–1535.
49. Litts KM, Messinger JD, Dellatorre K, Yannuzzi LA, Freund KB, Curcio CA. Clinicopathological correlation of outer retinal tubulation in age-related macular degeneration [published online ahead of print March 5, 2015]. *JAMA Ophthalmol*. doi: 10.1001/jamaophthalmol.2015.126.
50. Sayegh RG, Simader C, Scheschy U, et al. A systematic comparison of spectral-domain optical coherence tomography and fundus autofluorescence in patients with geographic atrophy. *Ophthalmology*. 2011;118:1844–1851.
51. Staurenghi G, Sadda S, Chakravarthy U, Spaide RF. Proposed lexicon for anatomic landmarks in normal posterior segment spectral-domain optical coherence tomography: the IN*OCT Consensus. *Ophthalmology*. 2014;121:1572–1578.
52. Ach T, Tolstik E, Messinger JD, Zarubina AV, Heintzmann R, Curcio CA. Lipofuscin redistribution and loss accompanied by cytoskeletal stress in retinal pigment epithelium of eyes with age-related macular degeneration. *Invest Ophthalmol Vis Sci*. 2015;56:3242–3252.
53. Moussa K, Lee JY, Stinnett SS, Jaffe GJ. Spectral domain optical coherence tomography-determined morphologic predictors of age-related macular degeneration-associated geographic atrophy progression. *Retina*. 2013;33:1590–1599.
54. Wu Z, Luu CD, Ayton LN, et al. Optical coherence tomography-defined changes preceding the development of drusen-associated atrophy in age-related macular degeneration. *Ophthalmology*. 2014;121:2415–2422.
55. Simader C, Sayegh RG, Montuoro A, et al. A longitudinal comparison of spectral-domain optical coherence tomography and fundus autofluorescence in geographic atrophy. *Am J Ophthalmol*. 2014;158:557–566.
56. Grunwald JE, Daniel E, Huang J, et al. Risk of geographic atrophy in the comparison of age-related macular degeneration treatments trials. *Ophthalmology*. 2014;121:150–161.
57. Marsiglia M, Boddu S, Chen CY, et al. Correlation between neovascular lesion type and clinical characteristics of non-neovascular fellow eyes in patients with unilateral neovascular age-related macular degeneration. *Retina*. In press.
58. Klein R, Davis MD, Magli YL, Segal P, Klein BEK, Hubbard L. The Wisconsin Age-Related Maculopathy Grading System. *Ophthalmology*. 1991;98:1128–1134.
59. Fleckenstein M, Schmitz-Valckenberg S, Adrion C, et al. Tracking progression using spectral domain optical coherence tomography in geographic atrophy due to age-related macular degeneration. *Invest Ophthalmol Vis Sci*. 2010;51: 3846–3852.
60. Holz FG, Bindewald-Wittich A, Fleckenstein M, Dreyhaupt J, Scholl HP, Schmitz-Valckenberg S. Progression of geographic atrophy and impact of fundus autofluorescence patterns in age-related macular degeneration. *Am J Ophthalmol*. 2007; 143:463–472.
61. Ahlers C, Gotzinger E, Pircher M, et al. Imaging of the retinal pigment epithelium in age-related macular degeneration using polarization-sensitive optical coherence tomography. *Invest Ophthalmol Vis Sci*. 2010;51:2149–2157.
62. Göbel AP, Fleckenstein M, Schmitz-Valckenberg S, Brinkmann CK, Holz FG. Imaging geographic atrophy in age-related macular degeneration. *Ophthalmologica*. 2011;226:182–190.
63. Green WR, Key SN III. Senile macular degeneration: a histopathologic study. *Trans Am Ophthalmol Soc*. 1977;75: 180–254.
64. Sarks SH, Arnold JJ, Killingsworth MC, Sarks JP. Early drusen formation in the normal and aging eye and their relation to age-related maculopathy: a clinicopathological study. *Br J Ophthalmol*. 1999;83:358–368.
65. Gass JDM. *Stereoscopic Atlas of Macular Diseases: Diagnosis and Treatment*. 4th ed. St. Louis: Mosby; 1997:.
66. Miller H, Miller B, Ryan SJ. The role of retinal pigment epithelium in the involution of subretinal neovascularization. *Invest Ophthalmol Vis Sci*. 1986;27:1644–1652.
67. Lafaut BA, Aisenbrey S, Vanden Broecke C, et al. Clinicopathological correlation of retinal pigment epithelial tears in exudative age related macular degeneration: pretear, tear, and scarred tear. *Br J Ophthalmol*. 2001;85:454–460.
68. Toth CA, Pasquale AC III, Graichen DF. Clinicopathologic correlation of spontaneous retinal pigment epithelial tears with choroidal neovascular membranes in age-related macular degeneration. *Ophthalmology*. 1995;102:272–277.
69. El-Emam S, Chhablani J, Barteselli G, et al. Correlation of spectral domain optical coherence tomography characteristics with visual acuity in eyes with subfoveal scarring after treatment for wet age-related macular degeneration. *Retina*. 2013;33:1249–1257.
70. Grossniklaus HE, Martinez JA, Brown VB, et al. Immunohistochemical and histochemical properties of surgically excised subretinal neovascular membranes in age-related macular degeneration. *Am J Ophthalmol*. 1992;114:464–472.
71. Dunaief JL, Dentchev T, Ying GS, Milam AH. The role of apoptosis in age-related macular degeneration. *Arch Ophthalmol*. 2002;120:1435–1442.
72. Bowes Rickman C, Farsiu S, Toth CA, Klingeborn M. Dry age-related macular degeneration: mechanisms, therapeutic targets, and imaging. *Invest Ophthalmol Vis Sci*. 2013;54: 68–80.
73. Buschini E, Piras A, Nuzzi R, Vercelli A. Age related macular degeneration and drusen: neuroinflammation in the retina. *Prog Neurobiol*. 2011;95:14–25.
74. Leuschen JN, Schuman SG, Winter KP, et al. Spectral-domain optical coherence tomography characteristics of intermediate age-related macular degeneration. *Ophthalmology*. 2013; 120:140–150.
75. Johnson NF, Foulds WS. Observations on the retinal pigment epithelium and retinal macrophages in experimental retinal detachment. *Br J Ophthalmol*. 1977;61:564–572.
76. Mandelcorn MS, Machemer R, Fineberg E, Hersch SB. Proliferation and metaplasia of intravitreal retinal pigment epithelium cell autotransplants. *Am J Ophthalmol*. 1975;80: 227–237.
77. Kuwabara T. Photic and photo-thermal effects on the retinal pigment epithelium. In: Zinn KM, Marmor MF, eds. *The Retinal Pigment Epithelium*. Cambridge: Harvard University Press; 1979:293–313.
78. Jaffe GJ, Irvine AR, Wood IS, Severinghaus JW, Pino GR, Haugen C. Retinal phototoxicity from the operating microscope. The role of inspired oxygen. *Ophthalmology*. 1988; 95:1130–1141.
79. Combadière C, Feumi C, Raoul W, et al. CX3CR1-dependent subretinal microglia cell accumulation is associated with cardinal features of age-related macular degeneration. *J Clin Invest*. 2007;117:2920–2928.
80. Bretillon L, Acar N, Seeliger MW, et al. ApoB100,LDLR-/- mice exhibit reduced electroretinographic response and cholesteryl esters deposits in the retina. *Invest Ophthalmol Vis Sci*. 2008;49:1307–1314.
81. Xu H, Chen M, Forrester JV. Para-inflammation in the aging retina. *Prog Retin Eye Res*. 2009;28:348–368.
82. Hoh Kam J, Lenassi E, Jeffery G. Viewing ageing eyes: diverse sites of amyloid Beta accumulation in the ageing mouse retina and the up-regulation of macrophages. *PLoS One*. 2010;5: e13127.
83. Ufret-Vincenty RL, Aredo B, Liu X, et al. Transgenic mice expressing variants of complement factor H develop AMD-

Investigative Ophthalmology & Visual Science

like retinal findings. *Invest Ophthalmol Vis Sci*. 2010;51:5878–5887.

84. Hu P, Herrmann R, Bednar A, et al. Aryl hydrocarbon receptor deficiency causes dysregulated cellular matrix metabolism and age-related macular degeneration-like pathology. *Proc Natl Acad Sci U S A*. 2013;110:E4069–E4078.
85. Chen X, Kezic J, Bernard C, McMenamin PG. Rd8 mutation in the Crb1 gene of CD11c-eYFP transgenic reporter mice results in abnormal numbers of CD11c-positive cells in the retina. *J Neuropathol Exp Neurol*. 2013;72:782–790.
86. Gupta N, Brown KE, Milam AH. Activated microglia in human retinitis pigmentosa, late-onset retinal degeneration, and age-related macular degeneration. *Exp Eye Res*. 2003;76:463–471.
87. Ma W, Coon S, Zhao L, Fariss RN, Wong WT. A2E accumulation influences retinal microglial activation and complement regulation. *Neurobiol Aging*. 2013;34:943–960.
88. Chen M, Forrester JV, Xu H. Dysregulation in retinal para-inflammation and age-related retinal degeneration in CCL2 or CCR2 deficient mice. *PLoS One*. 2011;6:e22818.
89. Hahn P, Qian Y, Dentchev T, et al. Disruption of ceruloplasmin and hephaestin in mice causes retinal iron overload and retinal degeneration with features of age-related macular degeneration. *Proc Natl Acad Sci U S A*. 2004;101:13850–13855.
90. Zhao C, Yasumura D, Li X, et al. mTOR-mediated dedifferentiation of the retinal pigment epithelium initiates photoreceptor degeneration in mice. *J Clin Invest*. 2011;121:369–383.
91. Campochiaro PA, Jerdan JA, Glaser BM. Serum contains chemoattractants for human retinal pigment epithelial cells. *Arch Ophthalmol*. 1984;102:1830–1833.
92. Kirchhof B, Sorgente N. Pathogenesis of proliferative vitreoretinopathy. Modulation of retinal pigment epithelial cell functions by vitreous and macrophages. *Dev Ophthalmol*. 1989;16:1–53.
93. Mukherjee S, Guidry C. The insulin-like growth factor system modulates retinal pigment epithelial cell tractional force generation. *Invest Ophthalmol Vis Sci*. 2007;48:1892–1899.
94. King JL, Guidry C. Vitreous IGFBP-3 effects on Muller cell proliferation and tractional force generation. *Invest Ophthalmol Vis Sci*. 2012;53:93–99.
95. Christenbury JG, Folgar FA, O'Connell RV, Chiu SJ, Farsiu S, Toth CA. Progression of intermediate age-related macular degeneration with proliferation and inner retinal migration of hyperreflective foci. *Ophthalmology*. 2013;120:1038–1045.
96. Folgar FA, Chow JH, Farsiu S, et al. Spatial correlation between hyperpigmentary changes on color fundus photography and hyperreflective foci on SDOCT in intermediate AMD. *Invest Ophthalmol Vis Sci*. 2012;53:4626–4633.
97. Burns RP, Feeney-Burns L. Clinico-morphologic correlations of drusen of Bruch's membrane. *Trans Am Ophthalmol Soc*. 1980;78:206–225.
98. Kerr JF, Wyllie AH, Currie AR. Apoptosis: a basic biological phenomenon with wide-ranging implications in tissue kinetics. *Br J Cancer*. 1972;26:239–257.
99. Galluzzi L, Bravo-San Pedro JM, Vitale I, et al. Essential versus accessory aspects of cell death: recommendations of the NCCD 2015. *Cell Death Differ*. 2015;22:58–73.
100. Kaneko H, Dridi S, Tarallo V, et al. DICER1 deficit induces Alu RNA toxicity in age-related macular degeneration. *Nature*. 2011;471:325–330.
101. Kim Y, Tarallo V, Kerur N, et al. DICER1/Alu RNA dysmetabolism induces Caspase-8-mediated cell death in age-related macular degeneration. *Proc Natl Acad Sci U S A*. 2014;111:16082–16087.
102. Malek G, Johnson LV, Mace BE, et al. Apolipoprotein E allele-dependent pathogenesis: a model for age-related retinal degeneration. *Proc Natl Acad Sci U S A*. 2005;102:11900–11905.
103. Marmorstein LY, McLaughlin PJ, Peachey NS, Sasaki T, Marmorstein AD. Formation and progression of sub-retinal pigment epithelium deposits in Efemp1 mutation knock-in mice: a model for the early pathogenic course of macular degeneration. *Hum Mol Genet*. 2007;16:2423–2432.
104. Fu L, Garland D, Yang Z, et al. The R345W mutation in EFEMP1 is pathogenic and causes AMD-like deposits in mice. *Hum Mol Genet*. 2007;16:2411–2422.
105. Garland DL, Fernandez-Godino R, Kaur I, et al. Mouse genetics and proteomic analyses demonstrate a critical role for complement in a model of DHRD/ML, an inherited macular degeneration. *Hum Mol Genet*. 2014;23:52–68.
106. Anderson DH, Mullins RF, Hageman GS, Johnson LV. A role for local inflammation in the formation of drusen in the aging eye. *Am J Ophthalmol*. 2002;134:411–431.
107. Zhao Z, Chen Y, Wang J, et al. Age-related retinopathy in NRF2-deficient mice. *PLoS One*. 2011;6:e19456.
108. Hollyfield JG, Bonilha VL, Rayborn ME, et al. Oxidative damage-induced inflammation initiates age-related macular degeneration. *Nat Med*. 2008;14:194–198.
109. Curcio CA, Messinger JD, Mitra AM, Sloan KR, McGwin G Jr, Spaide R. Human chorioretinal layer thicknesses measured using macula-wide high resolution histological sections. *Invest Ophthalmol Vis Sci*. 2011;52:3943–3954.
110. Rudolf M, Clark ME, Chimento M, Li C-M, Medeiros NE, Curcio CA. Prevalence and morphology of druse types in the macula and periphery of eyes with age-related maculopathy. *Invest Ophthalmol Vis Sci*. 2008;49:1200–1209.
111. Bird AC, Phillips RL, Hageman GS. Geographic atrophy: a histopathological assessment. *JAMA Ophthalmol*. 2014;132:338–345.
112. Monés J, Biarnes M, Trindade F. Hyporeflective wedge-shaped band in geographic atrophy secondary to age-related macular degeneration: an underreported finding. *Ophthalmology*. 2012;119:1412–1419.
113. Grossniklaus HE, Wilson DJ, Bressler SB, et al. Clinicopathologic studies of eyes that were obtained postmortem from four patients who were enrolled in the submacular surgery trials: SST Report No. 16. *Am J Ophthalmol*. 2006;141:93–104.
114. Hwang JC, Chan JW, Chang S, Smith RT. Predictive value of fundus autofluorescence for development of geographic atrophy in age-related macular degeneration. *Invest Ophthalmol Vis Sci*. 2006;47:2655–2661.
115. Smith RT, Gomes NL, Barile GR, Busuioc M, Lee N, Laine AF. Lipofuscin and autofluorescence metrics in progressive STGD. *Invest Ophthalmol Vis Sci*. 2009;50:3907–3914.
116. Curcio CA, Presley JB, Millican CL, Medeiros NE. Basal deposits and drusen in eyes with age-related maculopathy: evidence for solid lipid particles. *Exp Eye Res*. 2005;80:761–775.
117. Lommatzsch A, Hermans P, Muller KD, Bornfeld N, Bird AC, Pauleikhoff D. Are low inflammatory reactions involved in exudative age-related macular degeneration? Morphological and immunhistochemical analysis of AMD associated with basal deposits. *Graefes Arch Clin Exp Ophthalmol*. 2008;246:803–810.
118. Karampelas M, Sim DA, Keane PA, et al. Evaluation of retinal pigment epithelium-Bruch's membrane complex thickness in dry age-related macular degeneration using optical coherence tomography. *Br J Ophthalmol*. 2013;97:1256–1261.
119. Farsiu S, Chiu SJ, O'Connell RV, et al. Quantitative classification of eyes with and without intermediate age-related macular degeneration using optical coherence tomography. *Ophthalmology*. 2014;121:162–172.
120. Marmorstein AD, Marmorstein LY, Sakaguchi H, Hollyfield JG. Spectral profiling of autofluorescence associated with

Investigative Ophthalmology & Visual Science

lipofuscin, Bruch's Membrane, and sub-RPE deposits in normal and AMD eyes. *Invest Ophthalmol Vis Sci*. 2002;43:2435–2441.

121. Biarnés M, Monés J, Trindade F, Alonso J, Arias L. Intra and interobserver agreement in the classification of fundus autofluorescence patterns in geographic atrophy secondary to age-related macular degeneration. *Graefes Arch Clin Exp Ophthalmol*. 2011;250:485–490.
122. Xu L, Blonska AM, Pumariega N, et al. Reticular macular disease is associated with multilobular geographic atrophy in age-related macular degeneration. *Retina*. 2013;33:1850–1862.
123. Steinberg RH, Wood I, Hogan MJ. Pigment epithelial ensheathment and phagocytosis of extrafoveal cones in human retina. *Philos Trans R Soc Lond B Biol Sci*. 1977;277:459–474.
124. Jones BW, Kondo M, Terasaki H, Lin Y, McCall M, Marc RE. Retinal remodeling. *Jpn J Ophthalmol*. 2012;56:289–306.
125. Ouyang Y, Heussen FM, Hariri A, Keane PA, Sadda SR. Optical coherence tomography-based observation of the natural history of drusenoid lesion in eyes with dry age-related macular degeneration. *Ophthalmology*. 2013;120:2656–2665.
126. Fleckenstein M, Schmitz-Valckenberg S, Lindner M, et al. The "diffuse-trickling" fundus autofluorescence phenotype in geographic atrophy. *Invest Ophthalmol Vis Sci*. 2014;55:2911–2920.
127. Yehoshua Z, de Amorim Garcia Filho CA, Nunes RP, et al. Systemic complement inhibition with eculizumab for geographic atrophy in age-related macular degeneration: the COMPLETE study. *Ophthalmology*. 2014;121:693–701.
128. Evans JB, Syed BA. New hope for dry AMD? *Nat Rev Drug Discov*. 2013;12:501–502.
129. Schwartz SD, Regillo CD, Lam BL, et al. Human embryonic stem cell-derived retinal pigment epithelium in patients with age-related macular degeneration and Stargardt's macular dystrophy: follow-up of two open-label phase 1/2 studies. *Lancet*. 2014;385:509–516.
130. Kliffen M, van der Schaft TL, Mooy CM, de Jong PT. Morphologic changes in age-related maculopathy. *Microsc Res Tech*. 1997;36:106–122.
131. Grossniklaus HE, Gass JD. Clinicopathologic correlations of surgically excised type 1 and type 2 submacular choroidal neovascular membranes. *Am J Ophthalmol*. 1998;126:59–69.
132. Gehrs KM, Anderson DH, Johnson LV, Hageman GS. Age-related macular degeneration–emerging pathogenetic and therapeutic concepts. *Ann Med*. 2006;38:450–471.
133. Fleckenstein M, Schmitz-Valckenberg S, Martens C, et al. Fundus autofluorescence and spectral domain optical coherence tomography characteristics in a rapidly progressing form of geographic atrophy. *Invest Ophthalmol Vis Sci*. 2011;52:3761–3766.
134. Young RW. Pathophysiology of age-related macular degeneration. *Surv Ophthalmol*. 1987;31:291–306.
135. Sarks JP, Sarks SH, Killingsworth MC. Morphology of early choroidal neovascularization in age-related macular degeneration: correlation with activity. *Eye*. 1997;11:515–522.
136. Sarks J, Tang K, Killingsworth M, Arnold J, Sarks S. Development of atrophy of the retinal pigment epithelium around disciform scars. *Br J Ophthalmol*. 2006;90:442–446.
137. Penfold PL, Killingsworth MC, Sarks SH. Senile macular degeneration. The involvement of giant cells in atrophy of the retinal pigment epithelium. *Invest Ophthalmol Vis Sci*. 1986;27:364–371.
138. Fleckenstein M, Charbel Issa P, Helb HM, et al. High-resolution spectral domain-OCT imaging in geographic atrophy associated with age-related macular degeneration. *Invest Ophthalmol Vis Sci*. 2008;49:4137–4144.
139. Michels S, Pircher M, Geitzenauer W, et al. Value of polarisation-sensitive optical coherence tomography in diseases affecting the retinal pigment epithelium. *Br J Ophthalmol*. 2008;92:204–209.
140. Gorczynska I, Srinivasan VJ, Vuong LN, et al. Projection OCT fundus imaging for visualising outer retinal pathology in non-exudative age-related macular degeneration. *Br J Ophthalmol*. 2009;93:603–609.
141. Schmitz-Valckenberg S, Fleckenstein M, Helb HM, Charbel Issa P, Scholl HP, Holz FG. In vivo imaging of foveal sparing in geographic atrophy secondary to age-related macular degeneration. *Invest Ophthalmol Vis Sci*. 2009;50:3915–3921.
142. Chiu SJ, Izatt JA, O'Connell RV, Winter KP, Toth CA, Farsiu S. Validated automatic segmentation of AMD pathology including drusen and geographic atrophy in SD-OCT images. *Invest Ophthalmol Vis Sci*. 2012;53:53–61.
143. Grossniklaus HE, Hutchinson AK, Capone Jr A, Woolfson J, Lambert HM. Clinicopathologic features of surgically excised choroidal neovascular membranes. *Ophthalmology*. 1994;94:1099–1111.
144. Dastgheib K, Green WR. Granulomatous reaction to Bruch's membrane in age-related macular degeneration. *Arch Ophthalmol*. 1994;112:813–818.
145. Hashimoto T, Harada T. Confocal scanning laser microscopic findings of excised choroidal neovascular membranes of age-related macular degeneration and their comparison with the clinical features. *Jpn J Ophthalmol*. 1999;43:375–385.
146. Grossniklaus HE, Cingle KA, Yoon YD, Ketkar N, L'Hernault N, Brown S. Correlation of histologic 2-dimensional reconstructional and confocal scanning laser microscopic imaging of choroidal neovascularization in eyes with age-related maculopathy. *Arch Ophthalmol*. 2000;118:625–629.
147. Hariri A, Nittala MG, Sadda SR. Outer retinal tubulation as a predictor of the enlargement amount of geographic atrophy in age-related macular degeneration. *Ophthalmology*. 2014;122:407–413.

Investigative Ophthalmology & Visual Science

Supplementary Material

Zanzottera, E. C., Messinger, J. D., Ach, T., Smith, R. T., Freund, K. B., Curcio, C. A.

The Project MACULA retinal pigment epithelium grading system for histology and optical coherence tomography in age-related macular degeneration

Methods

Tissue Preparation

We evaluated eyes recovered from non-diabetic white donors for research by the Alabama Eye Bank (1995-2012). Median death-to-preservation time was 3:49 hours (range, 0:40-11:40 hours). Eyes were preserved by immersion in 1% paraformaldehyde and 2.5% glutaraldehyde in 0.1M phosphate buffer following anterior segment excision. When accessioned, eyes underwent *ex vivo* color photography. [39] When processed, eyes underwent *ex vivo* infrared reflectance imaging, 488 nm and 787 nm autofluorescence, and SDOCT volume scans (Spectralis, Heidelberg Engineering). [45]

Donor eyes with gross macular appearance consistent with AMD and lacking other chorioretinal macular pathology were processed. An 8-mm diameter full eye-wall punch centered on the fovea was trephined, post-fixed by osmium tannic acid paraphenylenediamine to accentuate extracellular lipid [46, 47] and embedded in epoxy resin

(PolyBed 812, Polysciences, Warrington PA). Sub-micrometer-thick sections [43, 48] were stained with toluidine blue, scanned with a microscope (BX51, Olympus, Center Valley, PA) equipped with a 40x 0.95 NA total internal reflection fluorescence objective and image-stitching software (CellSens; Olympus, Center Valley, PA). Digital sections (visible at http://projectmacula) were used for annotating morphology and thicknesses using custom ImageJ plug-ins (http://rsbweb.nih.gov/ij/). Sections were also photodocumented with a 60X oil-immersion objective (numerical aperture = 1.4) and digital camera (XC10, Olympus) and reviewed at 1900X on a monitor. Sections were initially annotated 2012-2013 by author CAC [8, 43] and re-annotated by author ECZ in 2014 to incorporate newly defined RPE grades.

Annotation and layer thickness measurements

The Superior section was the longest possible near the ring of high rod density (3-5 mm superior to the foveal center). [49] The Central section contained fovea, parafovea, and perifovea, and the Superior section contained only perifovea [50]. The nominal sampling scheme contained 13 locations in the Superior section and 25 in Central, from 3500 µm nasal to 3500 µm temporal to the fovea. The Central section contained more locations to capture features dependent on steep gradients of foveal neuronal cell density. The number of sampling locations varied among eyes, because 1/13 GA eyes and 3/39 CNV eyes had only a Central section, retinal detachment sometimes precluded use of section ends, and Superior sections, being chords of the circular tissue punch, were shorter than Central sections, which were diameters. Locations in detached neurosensory retina, which shrank more than RPE-choroid-sclera, were digitally adjusted to match.

Definitions of RPE cells, RPE-derived cells, and the RPE layer are given in the main text. If BLamD was not present, then there was no RPE layer, and attributing scars to sub-retinal or sub-RPE spaces required examination of surrounding tissue. We did not determine whether

vessels in fibrovascular scars originated in choroid or retinal circulation.

The procedure for measuring the thickness of epithelial RPE is given in the main text. The non-epithelial component of *Shedding* was not measured. The non-epithelial components of *Sloughed* and *Intraretinal* (i.e., individual desquamated cells) were measured only if they contacted the epithelial component. *Dissociated* RPE was not measured. We measured non-epithelial *Entombed* RPE when cells formed a continuous layer inside the scar, and where layered with other cells and fluid, only those cells closest to BLamD were measured. We did not measure a hyalinized envelope, if present.

Early BLamD is palisade-like, located close to BrM, has noticeable lipoprotein-derived debris within it, and appears in all BLamD. Late BLamD is scalloped (convex toward the RPE), located close to the RPE, has little lipoprotein-derived debris within it, and appears only in thick BLamD. BLamD was measured perpendicular to its outer extent if detached from BrM by sub-RPE scar or basal linear deposits. The latter are diffuse, gray-staining, lipid-rich soft drusen material between the RPE basal lamina and the inner collagenous layer of BrM; these were not measured.

Supplementary Table 1: Demographics of study eyes*					
Diagnosis	**# eyes**	**# donors**	**Gender (F:M)**	**Mean age, years (± SD)**	***Ex vivo* imaging and histology**
Geographic atrophy	13	12	8:4	85.6 ± 4.9	3 unilobular; 10 multilobular - 7 foveal affected; 6 foveal spared (Two fellow eyes had almost identical fovea-sparing lesions.)
Choroidal neovascularization	39	39	25:14	85.4 ± 7.2	37 CNV in foveola: 25 sub-retinal+sub-RPE scar; 4 sub-retinal scar, 5 sub-RPE scar; 1 sub-retinal scar+sub-RPE NV; 2 sub-RPE NV; 2 CNV extra-foveola: sub-RPE scar
Total	52	51			

* For 22 donors with clinical histories, the median time between the last clinic visit and death was 22.6 months (range, 2.1-106.1 months). No chorioretinal pathology except AMD was present. In all eyes a foveal depression could be detected even if the disease involved the fovea. The foveola was defined as 500 μm in diameter. [50]
CNV= choroidal neovascularization; NV= neovascularization; RPE= retinal pigment epithelium.

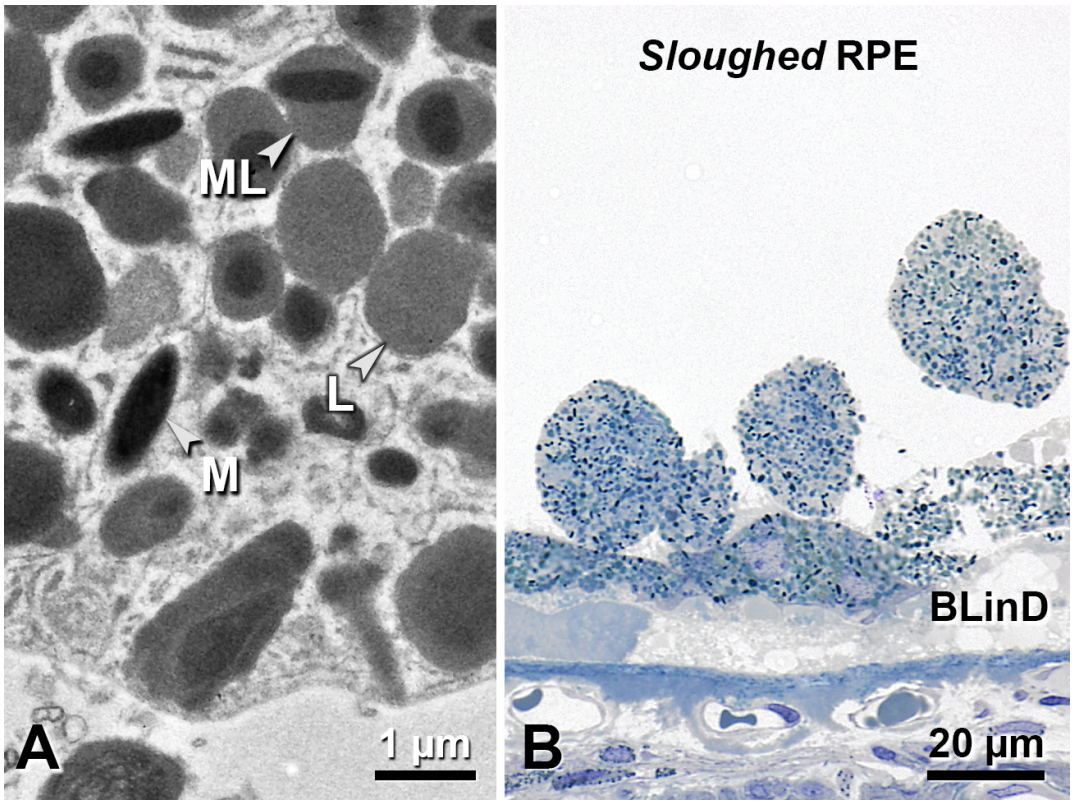

Supplementary Figure 1. RPE morphology and granules.

A. Transmission electron microscopy distinguishes definitively between lipofuscin (L), melanolipofuscin (MLF), and melanosomes (M) in desquamated RPE of an 85-year-old woman with early AMD. **B.** Sub-micrometer epoxy resin section, toluidine blue stain [48] in an 88-year-old woman with early AMD. Essentially an electron microscopy tissue preparation viewed by light microscopy, this preparation shows RPE granules clearly and is recommended for histology-OCT imaging comparisons. [146] *Sloughed* RPE consists of desquamated spherical cells internal to an epithelial layer, which in turn overlies basal linear deposit (BLinD). Desquamated cells with spindle-shaped melanosomes and numerous lipofuscin granules resemble the epithelial cells in granule types, sizes, packing density, and staining properties.

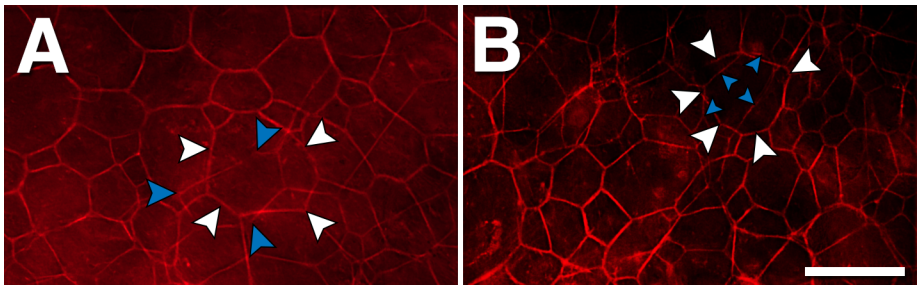

Supplementary Figure 2: Cytoskeleton of Bilaminar RPE.

A, B: RPE cells are delineated by their cytoskeleton. In each panel, two different RPE cytoskeleton layers are visible. Each individual layer is organized as a monolayer of multiple RPE cells. The arrowheads highlight the superimposed cytoskeleton of two RPE cells of slightly different sizes and orientations (blue and white arrowheads), which are lying upon each other. The RPE mosaic around *Bilaminar* was intact. Images were captured as part of a larger survey of RPE autofluorescence and cytoskeletal changes in aging and AMD [92]. Donor: 86 year-old female, neovascular AMD. Alexa647-phalloidin label. Scale bar: 50 µm.

Appendix: Key to Figures at http://projectmacula

Figure 2 RPE Grading System

A) *Non-uniform* RPE (RPE1): Section 2007012R-85F-4025, Eccentricity 2210 (perifovea).

B) *Very non-uniform* RPE (RPE2): Section 2005025R-88F-3950, Eccentricity -2590 (perifovea).

C) Non-epithelioid *Dissociated* RPE (RPE7) : Section 2007003R-94-F-3550 Neovascular AMD, Eccentricity 1500 (perifovea).

D) *Shedding* RPE (RPE2B): Section 2007012R-85F-4025, Eccentricity 670 (parafovea).

E) *Intraretinal* RPE (RPE3): Section 2006001R-79M-3875, Eccentricity -800 (parafovea).

F) Non-epithelioid *Entombed* layer (RPE6): Section 0099028L-87-F-4075, Late exudative ARM, Eccentricity 2000 (perifovea).

G) *Sloughed* RPE (RPE2A): Section2011013R-95M-3975, Eccentricity 700 (parafovea).

H) RPE *Atrophy with BLamD* (RPE4): Section 2011013R-95M-2000, Eccentricity -1025 (perifovea).

I) *Bilaminar* RPE (RPE2L): Section 2000020R-85F-3975, Eccentricity -2000 (perifovea).

J) *Vacuolated* RPE (RPE2V): Section 2009001L-87M-2000, Eccentricity -1500 (perifovea).

K) RPE *Atrophy without BLamD* (RPE5): Section 2011017R-83F-4000, Eccentricity -2720 (perifovea-peripapillary).

Figure 3 *Dissociated* RPE

A) Section 2008003L-96F-4100, Eccentricity 1790 (perifovea).

B) Section 2011017R-83F-4000, Eccentricity 260 (parafovea).

C) Section 2000020R-85F-3975, Eccentricity -600 (parafovea).

D) Section 2011013R-95M-2000, Eccentricity -2800 (perifovea).

Figure 4 *Entombed* RPE

A) Section 0099028L-87F-4075, Eccentricity -1850 (perifovea)

B) Section 2003037R-77M-3975, Eccentricity 850 (parafovea)

C) Section 2000003R-93F-2000, Eccentricity 2000 (perifovea)

D) Section 0099076L-77F-2000, Eccentricity -1500 (perifovea)

Figure 7 Clinicopathologic correlation

Not currently online.